Radiation Measurements 193 (2026) 107656

Contents lists available at ScienceDirect

Radiation Measurements

journal homepage: www.elsevier.com/locate/radmeas

Review

Scintillators in the search for neutrinoless double-beta decay: Technologies, status, and prospects☆

S. Dell'Oro, L. Gironi *

University of Milano-Bicocca, Milano, 20126, Italy
INFN, Sezione di Milano-Bicocca, Milano, 20126, Italy

ARTICLE INFO

Keywords:
Neutrinoless double-beta decay
Neutrino
Detectors

ABSTRACT

Neutrinoless double-beta decay ($0\nu\beta\beta$) is a key process for addressing fundamental questions about physics beyond the Standard Model and neutrino physics. Motivated by these goals, an extensive research effort has produced a wide range of increasingly sophisticated experimental approaches. Among the most widely adopted technologies are scintillators, in all their forms. Scintillators offer flexible detector configurations, high radiopurity, good detector performance and scalability to large mass of candidate isotopes. In many experiments, scintillators serve as primary detection media or are coupled with dual-readout schemes, such as light+heat or light+ionization, that greatly enhance background rejection and overall sensitivity. This review provides a comprehensive overview of scintillating technologies used in the search for $0\nu\beta\beta$, discussing their operating principles, the main experimental implementations, and the prospects for next-generation detectors.

Contents

1. Introduction 2
2. Neutrinoless double-beta decay 2
3. Search for $0\nu\beta\beta$ 3
   3.1. Experimental sensitivity 3
      3.1.1. Zero-background regime 3
      3.1.2. Finite-background regime 3
4. Present status 4
5. Increasing the sensitivity 5
   5.1. Active mass 5
   5.2. Background and energy resolution 5
   5.3. Future searches 5
6. Scintillators for $0\nu\beta\beta$ 6
   6.1. Solid scintillators 6
      6.1.1. Scintillation-only readout crystal detectors 6
      6.1.2. AURORA 6
      6.1.3. CANDLES-III 7
      6.1.4. Dual-readout detectors: scintillating bolometers 7
      6.1.5. CUPID 8
      6.1.6. AMoRE 8
   6.2. Liquid scintillators 9
      6.2.1. Loaded liquid scintillator detectors 9
      6.2.2. KamLAND-Zen & KamLAND2-Zen 9
      6.2.3. SNO+ 10
      6.2.4. Other loaded-LS experiments 10
      6.2.5. LS as active veto 10

☆ This article is part of a Special issue entitled: 'Scintillators Applications' published in Radiation Measurements.

* Corresponding author at: University of Milano-Bicocca, Milano, 20126, Italy.
E-mail address: luca.gironi@unimib.it (L. Gironi).

https://doi.org/10.1016/j.radmeas.2026.107656
Received 30 November 2025; Received in revised form 28 January 2026; Accepted 24 February 2026
Available online 27 February 2026
1350-4487/© 2026 The Authors. Published by Elsevier Ltd. This is an open access article under the CC BY license (http://creativecommons.org/licenses/by/4.0/).

6.3. Xenon TPCs 11
6.3.1. EXO-200 & nEXO 11
6.3.2. NEXT 12
6.3.3. AXEL 12
6.3.4. PandaX 12
6.3.5. XLZD 12
6.4. Novel techniques 12
6.4.1. Nanocomposite scintillators 12
6.4.2. Hybrid & opaque scintillators 13
7. Conclusions 13
CRediT authorship contribution statement 14
Declaration of Generative AI and AI-assisted technologies in the writing process 14
Declaration of competing interest 14
Data availability 14
References 14

1. Introduction

In 1930, W. Pauli postulated the existence of an electrically neutral, half-spin particle as a "desperate remedy" to preserve energy conservation in beta decays (Pauli, 1930). This particle was later named *neutrino* by E. Amaldi, as the Italian diminutive of the nuclear *neutrone* (neutron) discovered by J. Chadwick in 1932. The term neutrino then became widely used and was adopted as the standard designation thanks to E. Fermi, who used it in formulating his theory of beta decay (Fermi, 1934).

From the very beginning, it was clear that the experimental observation of the neutrino would be extremely challenging, as its mean free path in solid matter is of the order of a light year (Bethe and Peierls, 1934). The availability of a huge neutrino flux was therefore crucial for its discovery. The first observation of a neutrino occurred in 1956, thanks to the experimental work of C. Cowan and F. Reines at the Savannah River nuclear power plant (Cowan et al., 1956); actually, the observation was not of a neutrino, but of an anti-neutrino (Reines and Cowan, 1956).

A major breakthrough in neutrino physics came with the discovery of lepton flavor non-conservation, i. e. processes in which the flavor of a neutrino – determined at production by the accompanying charged lepton (electron, muon, or tau) – changes as it travels. The first indications emerged in the late 1960s, when a deficit was observed in the flux of solar neutrinos (Davis et al., 1968). It took nearly three decades to resolve this puzzle, ultimately confirming that the phenomenon, first proposed by B. Pontecorvo in 1957 (Pontecorvo, 1957), was that of "oscillations".

Currently, much of our understanding of neutrino mass comes from neutrino oscillation experiments. Oscillation experiments have now determined the mixing angles and mass splittings with subpercent precision (Capozzi et al., 2025), and are expected to determine the mass ordering in the near future (Abusleme et al., 2022; Abe et al., 2015; Abi et al., 2020). However, they are unable to probe the absolute value or the nature of the neutrino mass.

To address these questions, neutrinoless double-beta decay ($0\nu\beta\beta$) remains a privileged channel of investigation. The search for $0\nu\beta\beta$ is driving significant efforts to develop experiments with unprecedented sensitivity to extremely rare processes, posing highly demanding and often conflicting requirements on the detectors. In particular, there is a need for large active masses containing tonne-scale amounts of the isotope of interest, while simultaneously reducing backgrounds below the levels achieved so far only in smaller setups. In this context, scintillators in their various forms – thanks to their flexibility and performance – can play a crucial role in the next, or even next-to-next, generation of experiments.

2. Neutrinoless double-beta decay

The $0\nu\beta\beta$ process was introduced in 1939 by Furry (1939), in analogy to the "double-beta disintegration" described by M. Goeppert-Mayer in 1935 as the simultaneous beta decay that could occur in nuclei where the single beta decay is suppressed (Goeppert-Mayer, 1935). However, unlike the latter – today called two-neutrino double-beta decay ($2\nu\beta\beta$) – the $0\nu\beta\beta$ process required the introduction of the new formalism for the description of fermions developed by E. Majorana in 1937 (Majorana, 1937), and the insight by G. Racah that this formalism could indeed be applied to neutrinos (Racah, 1937). In the case of $0\nu\beta\beta$, no neutrinos are emitted and the transition takes the simple form

$$(A, Z) \rightarrow (A, Z+2) + 2e^{-}. \tag{1}$$

The most evident feature of Eq. (1) is the two-unit violation of lepton number, with the creation of a pair of electrons. The observation of $0\nu\beta\beta$ would therefore represent a clear signature of physics beyond the Standard Model and demonstrate that lepton number is not an exact symmetry. This, in turn, could support theoretical frameworks in which leptons play a role in generating the matter–antimatter asymmetry in the universe (Fukugita and Yanagida, 1986).

Among the possible explanations for the $0\nu\beta\beta$ process, the greatest interest certainly focuses on the neutrino mass mechanism (Dell'Oro et al., 2016). In order for ordinary neutrinos to be the mediators of the transition, two conditions must be simultaneously satisfied. Neutrinos must have non-zero mass and be Majorana particles. While the former has been clearly demonstrated, as the observation of neutrino oscillations proves a non-zero value for at least two of the neutrino mass eigenstates, the latter is actually being probed by the search for $0\nu\beta\beta$ itself.

The neutrino mass enters the $0\nu\beta\beta$ through the so-called *effective Majorana mass*, $m_{\beta\beta}$, the mass term (of Majorana type) that violates the lepton number in the Lagrangian density describing the neutrino charged-current interactions. Conventionally, $m_{\beta\beta}$ is parametrized using the same mixing matrix that connects the different neutrino flavors in oscillations – the PMNS matrix, named after B. Pontecorvo, Z. Maki, M. Nakagawa, and S. Sakata, who developed the theory – convoluted by the phases that describe the Majorana fields of the neutrino, two of which are physical and cannot be rotated out. Namely,

$$m_{\beta\beta} = \left| \sum_{i=1,2,3} e^{i\alpha_i} \left| U_{ei}^2 \right| m_i \right|. \tag{2}$$

We expect the amplitude of $0\nu\beta\beta$ to be proportional to $m_{\beta\beta}$, while the decay width (or the inverse half-life) is proportional to its squared modulus. By including the phase-space factor and the nuclear matrix element, which account for the fact that the process takes place within a nucleus, we can thus factorize:

$$\left(T_{1/2}^{0\nu}\right)^{-1} = G_{0\nu} \left| M_{0\nu} \right|^2 \left(\frac{m_{\beta\beta}}{m_e} \right)^2. \tag{3}$$

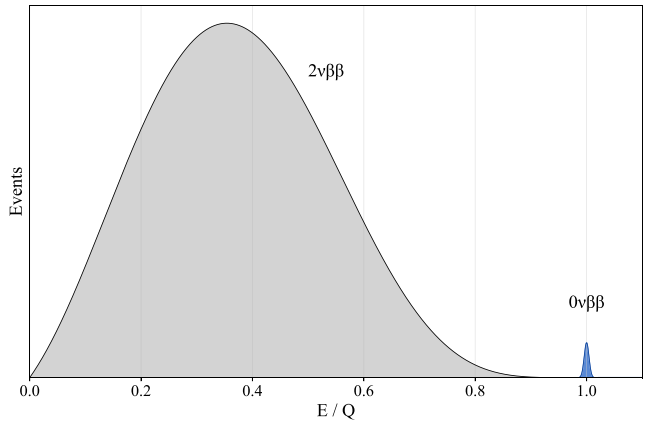


Fig. 1. Two-electron spectra of $2\nu\beta\beta$ and $0\nu\beta\beta$ (with arbitrary normalization). The $2\nu\beta\beta$ exhibits a continuous energy spectrum extending from zero up to $Q_{\beta\beta}$, as a fraction of the decay energy is carried away by the undetected neutrinos. In $0\nu\beta\beta$, the full kinetic energy of the emitted electrons is deposited in the detector; hence, the result is a monochromatic peak at $Q_{\beta\beta}$, whose width is determined by the detector energy resolution.

Eq. (3) connects the experimental observable in $0\nu\beta\beta$ searches to the information on the neutrino mass. A measurement of $T^{0\nu}_{1/2}$ can be translated into a value of $m_{\beta\beta}$, while a lower limit on $T^{0\nu}_{1/2}$ can be converted into an upper limit on $m_{\beta\beta}$. In practice, due to theoretical uncertainties in the computation of $G_{0\nu}$ (known to within a few percent (Kotila and Iachello, 2012)) and especially $M_{0\nu}$, which is affected by much larger uncertainties – up to a factor of a few (Agostini et al., 2023) – an experimental value or limit on $T^{0\nu}_{1/2}$ actually corresponds to a range of $m_{\beta\beta}$.

3. Search for $0\nu\beta\beta$

From an experimental point of view, the searches for $0\nu\beta\beta$ rely on detecting the two-electron signal. Since the energy of the recoiling nucleus is negligible, the total kinetic energy of the two electrons practically equals the total energy released in the nuclear transition (usually referred to as the Q-value, $Q_{\beta\beta}$). This monochromatic signal serves as the primary signature for all experiments (Fig. 1).

Despite its very distinctive signature, $0\nu\beta\beta$ remains challenging to observe due to its extreme rarity. The peak of interest lies in an energy range of a few MeV, where events from natural radioactivity occur on time scales many orders of magnitude shorter than the signal being searched for. Moreover, the $2\nu\beta\beta$ produces a continuous energy that extends up to $Q_{\beta\beta}$; in this case a fraction of the decay energy is carried away by the neutrinos, which are undetected. The $2\nu\beta\beta$ component is an unavoidable contribution to the statistics, originating from the same isotope of interest, and is characterized once more by a half-life orders of magnitude shorter than that of $0\nu\beta\beta$.

The choice of a suitable isotope (Table 1) is the first point to address. The outcome affects not only the background but also, directly or indirectly, all experimental parameters, starting with the detection technique, since the isotope of interest must be integrable into a functioning detector. Maximizing sensitivity is what ultimately drives the choice of the isotope-detector combination. An essential consideration is that, while $T^{0\nu}_{1/2}$ is the directly measurable quantity, it is $m_{\beta\beta}$ that carries the information on the neutrino mass. Since the two are connected through Eq. (3) via $G_{0\nu}$ and $M_{0\nu}$, these theoretical parameters must also be considered in the selection process. An experiment using a given isotope might result less performant than another from the purely experimental point of view, yet still yield a more stringent limit on the neutrino mass.

3.1. Experimental sensitivity

As stated, the measurable parameter in the search for $0\nu\beta\beta$ is the half-life of the transition, which can be extracted from the number of decays $n_{\beta\beta}$ detected in the region of interest (ROI) around $Q_{\beta\beta}$ as

$$T^{0\nu}_{1/2} = \ln 2 \; \varepsilon \; \frac{N_{\beta\beta}}{n_{\beta\beta}} \; T \tag{4}$$

after observing $N_{\beta\beta}$ $0\nu\beta\beta$-emitting nuclei over a time interval T, where ε accounts for the detection efficiency. In order to maximize detection efficiency, most experiments employ detectors whose active mass simultaneously serves as $0\nu\beta\beta$ source. This configuration also ensures that the emitted electrons deposit their full energy within the detector, thereby optimizing the energy resolution.

If no peak is detected in the experimental search, it is convenient to define the sensitivity, $S^{0\nu}_{1/2}$, either as the half-life limit corresponding to the minimum observable signal or as the half-life limit corresponding to the maximum background fluctuation. We designate the former as the *exclusion sensitivity* (rejecting a test signal under the assumption of background-only counts) and the latter as the *discovery sensitivity* (rejecting the background-only hypothesis). In the following, we will refer to the exclusion sensitivity when discussing $S^{0\nu}_{1/2}$.

3.1.1. Zero-background regime

When the active mass of the detector and the $0\nu\beta\beta$ source coincide, $N_{\beta\beta}$ can be expressed as

$$N_{\beta\beta} = M \; \frac{x \; \eta \; N_A}{A} \tag{5}$$

where M is the detector mass, x is the stoichiometric multiplicity of the element containing the candidate isotope, η is the isotopic abundance, N_A is Avogadro's number, and A is the molecular mass of the compound.

In the ideal scenario of experiments free from spurious events in the ROI, the experimental sensitivity then reads simply:

$$S^{0\nu}_{1/2} = \ln 2 \; \varepsilon \; \frac{x \; \eta \; N_A}{A} \; \frac{M \; T}{n_B} \tag{6}$$

where n_B is a constant determined by the chosen confidence level. The most striking feature of Eq. (6) is that it scales linearly with the product $M \; T$, commonly referred to as the *exposure*.

3.1.2. Finite-background regime

Current experiments usually exhibit spurious events in the ROI, hereafter referred to as background. If we assume the background to be proportional to the detector mass – as in the case of, e. g., internal contamination or cosmic radiation – the statistical fluctuation that determines $S^{0\nu}_{1/2}$ follows Poisson statistics. Its value (at 68% C. L.) is thus

$$n_B = \sqrt{M \; T \; B \; \Delta} \tag{7}$$

where B is the background level per unit mass, energy, and time (typically reported in [counts keV^{-1} kg^{-1} yr^{-1}]), and Δ is the full width at half maximum (FWHM) energy resolution. Therefore, the sensitivity now scales with the square root of the exposure

$$S^{0\nu}_{1/2} = \ln 2 \; \varepsilon \; \frac{x \; \eta \; N_A}{A} \; \sqrt{\frac{M \; T}{B \; \Delta}} \quad (68\% \text{ C. L.}). \tag{8}$$

In its simplicity, Eq. (8) has the advantage of highlighting the key experimental parameters—mass, measuring time, isotopic abundance, background level, energy resolution, and detection efficiency. This makes it straightforward to understand where to act to optimize the design of a $0\nu\beta\beta$ experiment in order to maximize sensitivity. The main requirements for a high-performance detector are:

- excellent energy resolution and the capability to extract the maximum possible information, such as electron energies and event topology; this also improves background discrimination;

Table 1
Properties of the most investigated isotopes for $0\nu\beta\beta$ searches, together with the current limits on $T^{0\nu}_{1/2}$ (including references), the calculated values of $G_{0\nu}$ (Kotila and Iachello, 2012) and $M_{0\nu}$ (Agostini et al., 2023), and the experimental techniques typically employed. In case more techniques are mentioned, the asterisk indicates which one has been used to achieve the reported limit on $T^{0\nu}_{1/2}$.

Isotope	Daughter	$Q_{\beta\beta}$[keV]	i. a. (%)	$T^{0\nu}_{1/2}$ (lim. inf.) [yr]	$G_{0\nu}$ [10^{-15} yr^{-1}]	$M_{0\nu}$	Technique(s)
^{48}Ca	^{48}Ti	4270	0.2	$5.8 \cdot 10^{22}$ (Umehara et al., 2008)	24.81		Scintillators*
							Bolometers
^{76}Ge	^{76}Se	2040	7.8	$1.9 \cdot 10^{26}$ (Acharya et al., 2026)	2.36	2.66 – 6.34	HPGe
^{82}Se	^{82}Kr	2995	9.2	$4.6 \cdot 10^{24}$ (Azzolini et al., 2022a)	10.16	2.72 – 5.30	Bolometers
^{100}Mo	^{100}Ru	3034	9.6	$2.9 \cdot 10^{24}$ (Agrawal et al., 2025a)	15.92	2.24 – 6.59	Bolometers
^{116}Cd	^{116}Sn	2802	7.5	$2.2 \cdot 10^{23}$ (Barabash et al., 2018)	16.70		Scintillators*
							Bolometers
^{130}Te	^{130}Xe	2527	33.7	$3.5 \cdot 10^{25}$ (D.Q. Adams et al., 2025)	14.22	1.79 – 6.41	Bolometers*
							Te dissolved in LS
^{136}Xe	^{136}Ba	2458	8.9	$3.8 \cdot 10^{26}$ (Abe et al., 2025)	14.58	1.11 – 4.77	Liquid/gas TPC
							Xe dissolved in LS*

- time stability and reliability – a user-friendly detector technology that requires minimal maintenance and allows for long, uninterrupted data-taking periods;
- very large mass, preferably isotopically enriched – today on the order of hundreds of kilograms or more;
- efficient and robust background suppression.

The transition from the finite-background to the zero-background regime occurs when the product in Eq. (7) approaches unity. Recent technological advances have made it possible to perform ultra-low-background experiments, where this condition can be met. However, it is essential to recognize that when the number of counts within the ROI is very small, the transition between the zero-background and finite-background regimes must be carefully evaluated on a case-by-case basis. Moreover, the zero-background condition can be maintained for a limited duration, often corresponding to just a fraction of the total experiment live time. These considerations illustrate why the computation of the sensitivity for an experiment is far from trivial, as one often does not fully fall within the cases expressed by Eq. (6) and (8), but rather lies in between.

4. Present status

The earliest searches for $0\nu\beta\beta$ date back to the late 1940s (Fireman, 1948); since then, dozens of experimental efforts have been carried out. Given the importance of the process and the progress achieved in neutrino physics, the number of experiments has increased steadily over the years. This has been accompanied by major technological advances, pushing established techniques to their limits and developing entirely new ones.

Despite extensive efforts, no experiment has yet observed $0\nu\beta\beta$. Experiments continue to push the boundaries of sensitivity, aiming to detect this elusive process or, at least, at further constraining the limit on the neutrino mass. Several reviews have already covered the long history of $0\nu\beta\beta$ searches (Barabash, 2011; Dell'Oro et al., 2016; Gómez-Cadenas et al., 2023); here, we focus only on recent/ongoing and future experiments, and even among these, only on a representative subset.

The current limits on the $0\nu\beta\beta$ half-life exceed 10^{22} yr for all isotopes listed in Table 1; The most stringent ones are larger than 10^{26} yr, and have been achieved for ^{76}Ge (Acharya et al., 2026) and ^{136}Xe (Abe et al., 2025). By converting the experimental constraints on $T^{0\nu}_{1/2}$ into bounds on $m_{\beta\beta}$, we can extract information on the neutrino mass. The latter quantity also enables comparison among searches performed with different isotopes, overcoming the experimental specificity.

A common representation shows $m_{\beta\beta}$ as a function of the lightest neutrino mass (Vissani, 1999). In this representation, each experimental limit (at a given C. L.) appears as a horizontal band, whose width is due the theoretical uncertainties in the nuclear physics entering the conversion through $M_{0\nu}$. The allowed regions for $m_{\beta\beta}$ are limited by the oscillation parameters. At the same time, for each value of the lightest neutrino mass, $m_{\beta\beta}$ can vary between a minimum and a maximum value (Dell'Oro et al., 2016) due to the presence of the unconstrained Majorana phases–physical parameters to be accounted for when describing the neutrino according to the Majorana formalism. It is important to notice that these allowed regions depend on the yet-unknown ordering of the neutrino mass eigenstates. The two scenarios of Normal and Inverted Hierarchy result are mutually incompatible, although they are usually represented together.

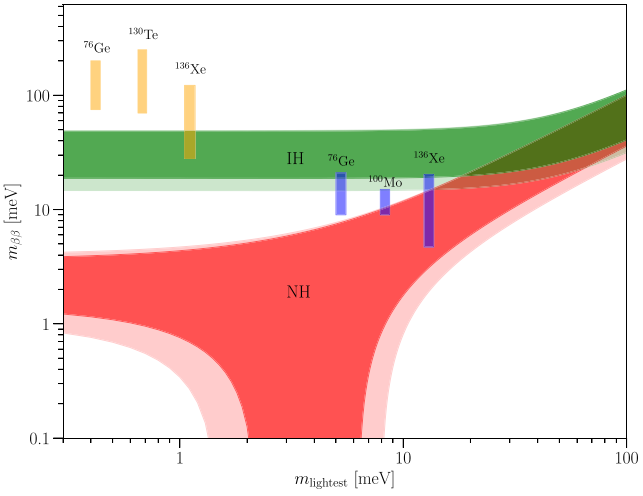


Fig. 2. Constraints on the effective Majorana mass as a function of the lightest neutrino mass. The darker areas are the $m_{\beta\beta}$ regions allowed by the oscillation experiments in the case of Normal Hierarchy and Inverted Hierarchy based on the best-fit parameters (Capozzi et al., 2025); the shaded regions correspond to the 3σ ranges. The orange boxes correspond to the limits on some of the isotopes in Table 1 from current and past experiments (Acharya et al., 2026; D.Q. Adams et al., 2025; Abe et al., 2025); the blue boxes refer to future searches from next-generation $0\nu\beta\beta$ experiments (Abgrall et al., 2021; Alfonso et al., 2025; Adhikari et al., 2022).

The result corresponding to the updated values of the oscillation parameters is shown in Fig. 2. The upper bounds on $m_{\beta\beta}$ from a few examples of current and future experiments (see the discussion in the next sections) are rendered as narrow boxes, although they actually correspond to horizontal bands. The values range from several tens to a few hundreds of meV for the current generation; in the most favorable theoretical scenarios, they allow probing a fraction of the so-called Inverted Hierarchy band, i. e. the region in that scenario where the value of $m_{\beta\beta}$ is practically independent of the mass of the lightest neutrino. Reaching about 10 meV, hence covering the Inverted-Hierarchy region, is the primary goal of the next generation of $0\nu\beta\beta$ experiments.

5. Increasing the sensitivity

As indicated by Eqs. (6) and (8), several experimental parameters determine the overall sensitivity to the $0\nu\beta\beta$ half-life and can be optimized in order to maximize it. Some of these parameters still offer significant margins for improvement, while others are unlikely to yield substantial gains. For instance, the live time is constrained by the practical impossibility of extending the data-taking beyond roughly ten years, already challenging due to the natural lifetime of instrumentation and the difficulty of maintaining software and interfaces over such long timescales. At best, we can aim to maximize the duty cycle, but this would result in less than a factor-of-two improvement compared to current values.

Conversely, acting on the active detector mass, background level, and energy resolution can significantly enhance the final sensitivity.

5.1. Active mass

The number of candidate nuclei undergoing $0\nu\beta\beta$ is arguably the most crucial parameter in this research. After all, without isotopes capable of undergoing $0\nu\beta\beta$, even the best energy resolution or lowest background levels would be meaningless.

As reported in Eq. (5), the number of nuclei under study is a fraction of the detector's active mass – the actual source of the decay – after accounting for chemistry, through the stoichiometric multiplicity of the compound, and for physics, through the isotopic abundance. The stoichiometric multiplicity is essentially fixed, since the structure and properties of the detector (electrical, magnetic, thermal, ...) depend on the material itself. In contrast, increasing the fraction of the isotope of interest does not affect the chemistry but enhances the signal rate and improves the signal-to-background ratio, as the total mass contributing to radioactive and cosmogenic backgrounds remains unchanged.

With the practical exception of ^{130}Te, the natural isotopic abundance of most $0\nu\beta\beta$ isotopes is generally too low to be experimentally viable (Table 1). It is therefore clear that selecting isotopes that can be enriched with relative ease represents a significant advantage for $0\nu\beta\beta$ experiments. Isotopic enrichment is nontrivial, and both its cost and difficulty depend strongly on the specific isotope; in any case, it can increase the material cost by up to two orders of magnitude (Biller, 2013). Most state-of-the-art experiments already employ isotopically enriched materials despite the significant technical and financial challenges of enrichment. In order to reach sensitivities to the $0\nu\beta\beta$ half-life greater than 10^{27} yr, the next-generation of experiments will require detector masses on the order of a tonne and isotopic enrichment above ~80% in the isotope of interest will be a crucial factor of the mass scalability process.

Finally, it is important to stress the role of the detection efficiency, which reduces the number of candidate nuclei from the total to the fraction whose energy release can actually be measured. Factors such as fiducialization of the detector volume or topological constraints in event selection can significantly decrease the effective active mass. These effects must therefore be carefully accounted for and optimized to maximize the number of nuclei under observation.

5.2. Background and energy resolution

In the case of $0\nu\beta\beta$, the background level in the region of interest is closely linked to the energy resolution. Every experiment searching for $0\nu\beta\beta$ will inevitably observe events from the allowed $2\nu\beta\beta$ mode, which produces a continuous spectrum extending up to $Q_{\beta\beta}$ (Fig. 1). The energy resolution determines the width of the region of interest around $Q_{\beta\beta}$, and thus whether background events – and which portion of the $2\nu\beta\beta$ spectrum – are included. Fig. 3 illustrates this effect by showing an energy spectrum around $Q_{\beta\beta}$convolved with different energy resolutions, ranging from a few per mil to some percent. In the latter case, any potentially visible peak is completely smeared out by the background.

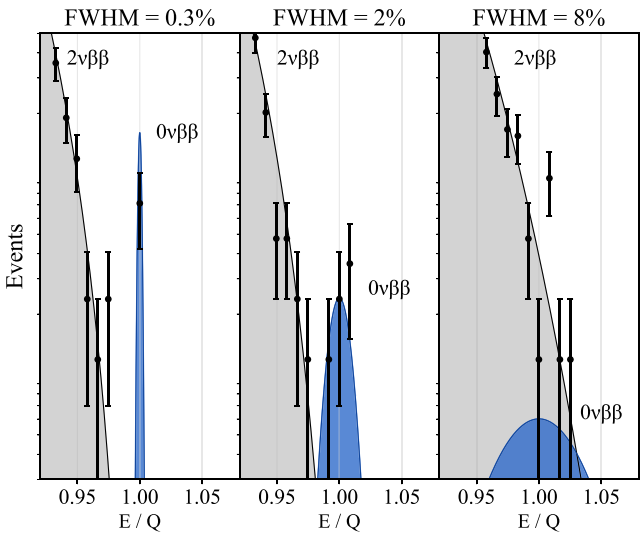


Fig. 3. Two-electron spectra around $Q_{\beta\beta}$for three detectors with different energy resolutions. In the high-energy-resolution case (left), the $0\nu\beta\beta$ contribution clearly emerges above the background, whereas in the low-energy-resolution case (right) it becomes indistinguishable from background fluctuations. Moreover, as the energy resolution degrades, an increasing fraction of $2\nu\beta\beta$ events extends beyond $Q_{\beta\beta}$, further raising the background level in the region of interest. Simulated data from Monte Carlo studies are overlaid to the spectra; these have been obtained by assuming an exposure of 5 t_{iso} for a year and a half-life of $3 \cdot 10^{27}$ yr for $0\nu\beta\beta$ and $2.4 \cdot 10^{21}$ yr for $2\nu\beta\beta$–case of ^{136}Xe. No additional background sources are included, in order to isolate the impact of the energy resolution; these could actually exist in real experiments, worsening the scenario.

In addition to $2\nu\beta\beta$, background events may arise from cosmic radiation, environmental radioactivity, and any process that produces an energy deposition comparable to that of $0\nu\beta\beta$. All $0\nu\beta\beta$ experiments are conducted in deep-underground laboratories and employ multiple layers of passive and active shielding around the detectors, which are constructed from carefully selected low-radioactivity materials. These requirements have driven, since the very beginning, the technological and strategic choices for the construction of detectors searching for $0\nu\beta\beta$. The next-generation of experiments, however, will face an entirely new level of complexity. To satisfy the condition in Eq. (7) for a tonne-scale detector operating over year-long periods with an energy resolution of the order of 10 keV, the background level must reach 10^{-4} counts keV^{-1} kg^{-1} yr^{-1} or lower. Achieving this will demand pushing existing technologies to unprecedented levels of radiopurity and background-rejection capability, in order to suppress what is commonly referred to as internal background (spurious events arising from the radioactive decays of contaminants within the detector itself), as well as external background (events originating from the radioactivity of the materials used in the construction of the detector, the shielding, or the surrounding environment). Depending on the detector type and configuration, complementary information to the energy deposition, such as the topology or the identification of the interaction type, will be essential to mitigate dominant background sources. Ultimately, the success of future searches will depend on how effectively these complementary approaches – material purity, detector design, and event characterization – will be integrated into a coherent experimental strategy.

5.3. Future searches

The next decades will see a major effort by the neutrino community to pursue increasingly sensitive searches for $0\nu\beta\beta$, as this investigation

addresses key questions in particle physics while offering a clear strategy for exploring the neutrino-mass parameter space. The goal will be to probe neutrino masses down to about 10 meV, thereby investigating a significant portion of the allowed mass region and fully covering the Inverted Hierarchy band, consistently with inputs from nuclear physics. In practice, this requires achieving experimental sensitivities of $T^{0\nu}_{1/2} \gtrsim 10^{27}$ yr.

The number of searches will be strongly limited by the substantial cost – both financial and in terms of time – of isotope procurement, as well as by the complexity and scale of the experiments given the size of the worldwide $0\nu\beta\beta$ community. A fundamental requirement will be demonstrating that a technology expected to operate in tonne-scale detectors – necessary for reaching the target sensitivity – is sufficiently mature. Most proposed future searches are upgrades of, or joint efforts among, existing experiments, led by groups that have already demonstrated the ability to operate high-performance detectors at current sensitivity levels and that present a realistic path toward improving performance and, in particular, suppressing backgrounds to approach the zero-background regime.

6. Scintillators for $0\nu\beta\beta$

Discussing scintillators for $0\nu\beta\beta$ searches actually means referring to a family of techniques rather than a single approach, each with specific strengths. A key distinction is between solid and liquid scintillators. Solid scintillators, especially when used with the combined heat+light readout, offer improved energy resolution and higher detection efficiency, making them well suited for a clear measurement of the $0\nu\beta\beta$ peak. Liquid scintillators (LS), on the other hand, inherently have lower resolution: should a signal show up in one of these experiments, it will be challenging to prove that it originates from $0\nu\beta\beta$, as such a signal will appear as a large excess, under which every other possible contribution must be carefully ruled out. However, liquid scintillators compensate with the ability to load very large masses of isotope. They are extremely effective for setting exclusion limits.

For ^{136}Xe, an extra possibility exists, namely liquid or gaseous xenon TPCs, which provide both low backgrounds and detailed event reconstruction.

6.1. Solid scintillators

Using scintillating crystals, measuring only the scintillation light with different light-sensor technologies is already sufficient to build a $0\nu\beta\beta$ detector. However, the most effective results have been obtained when light-collection information is used as a parallel channel to heat-signal measurement in bolometric experiments. In these cases, the dual readout enables identification of the interaction type and thus supports background suppression.

6.1.1. Scintillation-only readout crystal detectors

Scintillating crystals have long been considered an attractive option for investigating $0\nu\beta\beta$ thanks to their flexibility in isotope choice, ease of use, and the low background levels they can achieve.

Many scintillators naturally host candidate nuclei for $0\nu\beta\beta$, providing access to a broad range of isotopes without the stringent constraints typical of other detection techniques. This flexibility also extends to light-collection methods, which can be optimized for the specific emission properties of each compound. Maximizing the light yield and collection efficiency can substantially improve the achievable energy resolution.

Crystal scintillators also allow for intrinsically low background levels owing to their high radiopurity. In addition, they offer powerful tools for mitigating residual background. The quenching described by Birks' empirical law (Birks, 1951) results in a lower light yield for α particles and nuclear recoils than for electrons; quenching factors for α particles as low as 0.2 (Tretyak, 2010) effectively remove the entire α-induced component from the region around $Q_{\beta\beta}$. Many scintillators further provide intrinsic α/β discrimination via pulse-shape analysis, which is particularly valuable for tagging α-β coincidences.

Arrays of scintillating crystals can be constructed in a compact setup with comparatively modest technological requirements and at relatively low cost, making them appealing for large-scale experiments.

These advantages have supported several past experiment. Two notable examples of $0\nu\beta\beta$ searches based on crystal scintillators are described in the following sections.

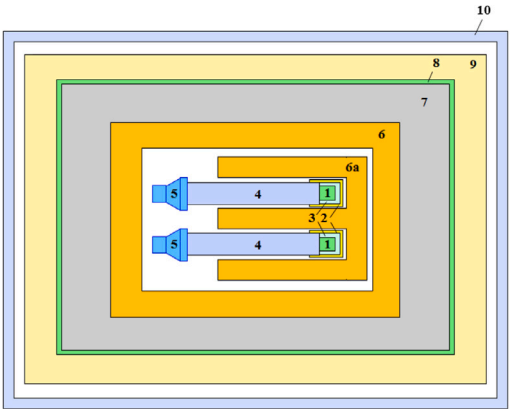


Fig. 4. Cross-sectional schematic of the Aurora setup. The $^{116}CdWO_4$ crystal scintillators (1) are mounted inside PTFE containers (2) filled with liquid scintillator (3) and coupled to PMTs (5) via quartz light guides (4). The passive shielding includes high-purity copper (6), an additional high-purity copper layer (6a), low-radioactivity lead (7), cadmium (8), polyethylene/paraffin (9), and an outer Plexiglas enclosure (10).
Source: Reprinted from Ref. Barabash et al. (2018).

6.1.2. AURORA

The AURORA detector consisted of a pair of cadmium tungstate ($CdWO_4$) crystals of ~580 g each, enriched in ^{116}Cd. The two crystals were produced from the same 1868 g boule grown using the low-thermal-gradient Czochralski technique (Barabash et al., 2011). The isotopic composition and trace impurities were measured via high-resolution ICP-MS, yielding an absolute abundance of 82.2% for ^{116}Cd, while the fraction of ^{113}Cd – a β emitter with half-life $\sim 8 \cdot 10^{15}$ yr – was reduced from its natural value of ~12% to ~2%.

The $0\nu\beta\beta$ search was carried out at the DAMA/R&D facility at Laboratori Nazionali del Gran Sasso (LNGS) between 2011 and 2017 (Barabash et al., 2018). Prior optical characterization of the scintillators showed good transmission in the 400–600 nm range, with an attenuation length of (31 ± 5) cm at 480 nm. The energy resolution at the 2615 keV γ-line of ^{208}Tl for the two detectors was 14.6(16.2)% FWHM, later improved to ~11.8(12.5)% after the crystals underwent an annealing cycle of 55 h at ~870 °C.

The complete experimental setup is shown in Fig. 4. To reduce background, the detectors were placed inside PTFE containers filled with liquid scintillator serving as an active veto. Light from both the crystals and the liquid scintillator was transported to the photomultipliers (PMTs) through quartz light guides. Additional shielding was provided by a layered polyethylene/paraffin + lead + copper structure. The entire setup was enclosed in a Plexiglas box and continuously flushed with high-purity nitrogen to remove environmental radon.

The analysis exploited the pulse-shape discrimination capabilities of $CdWO_4$ which, combined with time-amplitude selection of fast ^{232}Th subchains, enabled the experiment to achieve a background level of 0.15 counts keV^{-1} kg^{-1} yr^{-1} in the region of interest.

After about four years of live-time (35 324 h), the extracted limit on the $0\nu\beta\beta$ decay of ^{116}Cd was $T^{0\nu}_{1/2} > 2.2 \cdot 10^{23}$ yr.

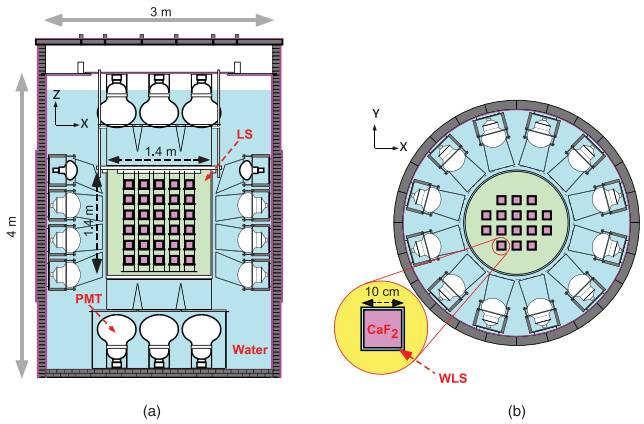


Fig. 5. Rendering of the CANDLES-III setup: side view (a) and top view (b), including a magnified detail of a CaF_2 module.
Source: Reprinted from Ref. Ajimura et al. (2021).

6.1.3. CANDLES-III

The CANDLES-III (CAlcium fluoride for the study of Neutrinos and Dark matters by Low Energy Spectrometer) experiment is the evolution of the search for $0\nu\beta\beta$ of ^{48}Ca from ELEGANT-VI (Umehara et al., 2008). CANDLES-III is located in the Kamioka underground laboratory (Japan) and presented its latest results in 2021. The detector comprises 96 modules arranged in 6 horizontal layers (Fig. 5). Each module consists of a 10-cm^3 cubic undoped CaF_2 crystal enclosed in a 3-mm-thick acrylic container filled with a 5-mm-thick layer of wavelength shifter (WLS) phase. The crystal mass is about 3 kg, for a total of 305 kg for the whole detector; this include ∼350 g of ^{48}Ca. The WLS phase consists of mineral oil in which Bis-MSB is dissolved at 0.1 g l^{-1} (Yoshida et al., 2009). The WLS converts the emission light of CaF_2, which peaks in the UV, into visible light, where the quantum efficiency of the PMTs is higher.

The structure of the WLS layer surrounding the CaF_2 crystals is crucial also because the detector is immersed in LS – 80% mineral oil, 20% pseudocumene, and WLSs (PPO at 1.0 g l^{-1} and Bis-MSB at 0.1 g l^{-1}) – which is not transparent to UV light. The LS is enclosed in a 1.4-m diameter, 1.4-m height vessel, in turn placed inside a water tank, together serving as an active shield, and observed by 62 PMTs. Outside the water tank, a lead shield and a B_4C sheet protect the setup from external gamma-ray and neutron backgrounds.

The technology in CANDLES-III is mature thanks to the validated performance of the CaF_2 crystals in the preliminary phases (CANDLES-I and CANDLES-II), which ultimately allowed the experiment to reach a background level of $\sim 10^{-3}$counts keV^{-1} kg^{-1} yr^{-1} in the region of interest. A close collaboration with the production company was crucial in order to define a strict validation protocol for the CaF_2 crystals. To minimize radioactive impurities, a three-stage selection process was implemented, starting from the screening of the raw CaF_2 powders via HPGe measurement. The selected powders were then melted and crystallized in a crucible, where a second selection was performed on samples cut from the resulting ingots. These samples were mounted on PMTs and tested for internal contamination in a low-radioactivity underground facility by dedicated delayed-coincidence of the Bi–Po subchains. Only then, crystals of nominal size were cut and polished from the qualified ingots, while those exceeding 100 μBq kg^{-1} were excluded.

The development of a dedicated calibration system using (n_γ) reactions allowed to estimate the resolution at the very-high $Q_{\beta\beta}$ of ^{48}Ca, yielding an average value of (5.7 ± 0.5)% FWHM (Iida et al., 2021). The results of the $0\nu\beta\beta$ search after a live-time of 130.4 days resulted in the limit of $T^{0\nu}_{1/2} > 2.7 \cdot 10^{22}$ yr for ^{48}Ca (Ajimura et al., 2021).

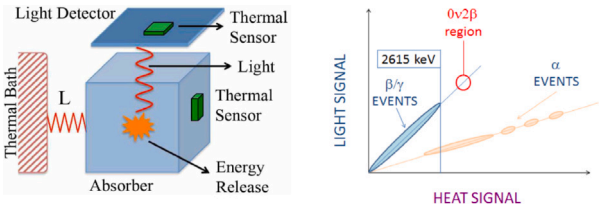


Fig. 6. (Left) Idealized sketch of a scintillating bolometer: a particle interaction deposits energy in the main absorber crystal produces both a heat and a light signal. Thermal sensors attached to both the absorber and the light detector measure the phonons (also the scintillation light is converted into a heat pulse). (Right) Illustration of particle identification through the combined use of heat and light signals, exploiting the differing light yields of α and β/γ particles.
Source: Reprinted from Ref. Alfonso et al. (2025).

A major limitation in CANDLES is the very low natural abundance of ^{48}Ca, which is ∼0.2%. Although ^{48}Ca is among the most produced $0\nu\beta\beta$ candidate isotopes – the world production is about 0.5 Mt per year – enrichment is currently not feasible on a large scale because calcium cannot be transformed into a gas. Strong effort by the CANDLES Collaboration is devoted to developing alternative enrichment strategies (Ogawa et al., 2023). At the same time, they are investigating the possibility of exploiting a double-readout technique, considering a CaF_2 scintillating-bolometer array (Tetsuno et al., 2020).

6.1.4. Dual-readout detectors: scintillating bolometers

Despite their strengths, large crystal-scintillator arrays have not yet reached their full potential. Their main limitation remains energy resolution, which still cannot compete with that of bolometric or HPGe-based searches, which is of a few per mille. Because the availability of the isotopes used in these detectors remains a crucial and challenging issue, the technique's flexibility cannot fully compensate for its lower performance. Improving resolution may require more advanced light detectors – e. g., Silicon drift detectors (SDDs) instead of PMTs – in combination with operation at lower temperatures (Bonvicini et al., 2014). These approaches could bring the resolution to the point where it is limited only by carrier statistics – namely, fluctuations in the number of produced optical photons – so that this contribution no longer represents a significant constraint. However, these proposals remain at the R&D stage.

Scintillating bolometers combine the features of scintillators with the excellent energy resolution of bolometers. This comes at the cost of ease of use: because these detectors are operated at cryogenic temperatures, they are significantly more complex to handle than standard scintillators. This added complexity can reduce the measurement live time and greatly complicate the construction of the experimental apparatus.

The working principle of scintillating bolometers is illustrated in Fig. 6. The detector is constructed by coupling a scintillating crystal to a germanium or silicon slab, the former acting as the main absorber and the latter as the light detector, with both operated as cryogenic calorimeters. When a particle interacts with the scintillating crystal, most of the deposited energy is converted into heat, while a smaller fraction produces scintillation light; the photons escaping the crystal are then collected by the light detector, where they are also converted into heat.

The resulting dual readout, heat+light, enables active, event-by-event particle identification. In particular, this discrimination capability allows cryogenic calorimeters to suppress background by orders of magnitude relative to purely calorimetric searches, thereby significantly enhancing experimental sensitivity. For these reasons, numerous research groups have been and still are actively working to optimize this technology on different compounds, such as $CdWO_4$ (Arnaboldi

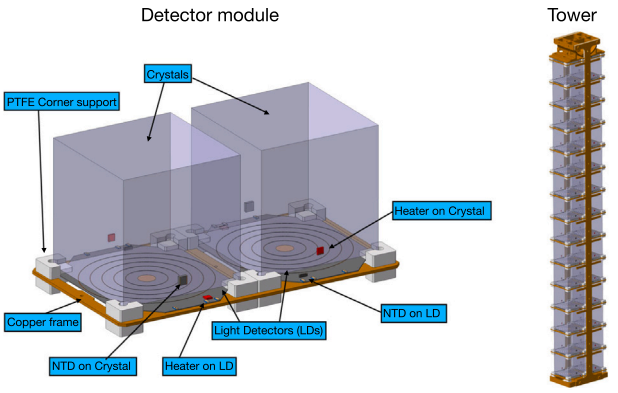


Fig. 7. (Left) Schematic view of a single CUPID floor: each of the two modules is composed of a LMO crystal and a Ge light detector with Al electrodes for the NTL amplification. Both LMO and Ge detectors are endowed with a NTD for the signal readout and a Si heater for the stabilization of the thermal gain. (Right) One of the 57 CUPID towers, consisting of 14 floors and 28 detector modules in total.
Source: Reprinted from Ref. Alfonso et al. (2025).

et al., 2010), ZnSe (Azzolini et al., 2022b) and $ZnMoO_4$ (Gironi et al., 2010). The most advanced efforts are represented by the future CUPID and AMoRE experiments, which will be described in the following sections. These next-generation detectors are both based on dual heat–light readout and share several key design principles, starting from the isotope, namely ^{100}Mo, selected for its high $Q_{\beta\beta}$ (about 3 MeV), and crystal compound, namely lithium molybdate (Li_2MoO_4, or LMO).

LMO is a highly promising material for scintillating bolometers. Advances in crystal growth – particularly low-thermal-gradient Czochralski and Bridgman techniques – now enable the production of large, mechanically robust boules with excellent optical quality. In terms of radiopurity, equally crucial for rare-event searches, intensive purification of the Li_2CO_3 and MoO_3 precursors can drive internal contaminants, such as ^{226}Ra and ^{228}Th, into the μBq kg^{-1} range in the final crystals (Alfonso et al., 2023).

Some challenges remain: potassium impurities and radium segregation during growth call for further optimization. In principle, crystallization inherently improves purity, so multiple crystallization cycles might help; each additional cycle, however, introduces material losses and substantially increases overall cost, since the MoO_3 must be enriched in ^{100}Mo. The price of $^{100}MoO_3$ is the dominant contribution to crystal production, making the minimization of material loss during growth and processing a central requirement. Post-growth processing is also demanding: annealing may be required to remove structural defects, and the ingot must be cut to its final geometry while avoiding mechanical damage, surface contamination, and further material loss. The finished crystals must satisfy bolometric performance criteria and, because LMO is slightly hygroscopic, polishing must be carried out with water-free methods in low-humidity environments. Humidity-resistant sealing and radiopure containers are also essential to ensure safe storage and transport.

Although overcoming these difficulties is challenging, they are being effectively addressed, with continuous progress in purification, growth, and material recovery. As a result, the performance of LMO crystals is steadily approaching the levels required for next-generation bolometric detectors.

6.1.5. CUPID

CUPID (CUORE Upgrade with Particle IDentification) builds upon the CUORE infrastructure at the Laboratori Nazionali del Gran Sasso (Italy). CUORE (Cryogenic Underground Observatory for Rare Events) is the largest cryogenic calorimeter array ever built, the culmination of nearly four decades of technological development and scientific measurements (Brofferio and Dell'Oro, 2018). The experiment has been in data-taking since 2017, searching for the $0\nu\beta\beta$ decay of ^{130}Te. The CUORE detector consists of an array of 988 TeO_2 crystals operated at approximately 10 mK, with a total mass of over 740 kg. Its energy resolution is excellent—only a few per mille at $Q_{\beta\beta}$; however, its main limitation remains the background level, around 10^{-2} counts keV^{-1} kg^{-1} yr^{-1} and dominated by α events (Adams et al., 2024). Being a pure (non-scintillating) calorimeter, CUORE cannot perform particle identification. As of 2025, CUORE has set a lower limit of $3.8 \cdot 10^{25}$ yr (90% C.,L.) on the half-life of ^{130}Te (D.Q. Adams et al., 2025).

Demonstrators at the kg scale have shown the ability to operate scintillating bolometer arrays effectively. CUPID-Mo operated 20 LMO crystals with a typical energy resolution of 5–7 keV FWHM at 2615 keV and demonstrated α/β discrimination at more than 3σ significance (Augier et al., 2022). Previously, CUPID-0, based on ZnSe crystals enriched in ^{82}Se, further validated the scalability of this approach, reaching $3.5 \cdot 10^{-3}$ counts keV^{-1} kg^{-1} yr^{-1}at $Q_{\beta\beta}$ (Azzolini et al., 2022a) (the Q-values for ^{82}Se and ^{100}Mo are close).

The CUPID baseline technology employs LMO crystals enriched in ^{100}Mo, read out with neutron-transmutation-doped (NTD) Ge thermistors for the heat channel and Ge-wafer light detectors acting as cryogenic calorimeters for the scintillation signal (Fig. 7). To collect the emitted light in scintillating bolometers, a Ge or Si wafer is commonly used: the photons depositing energy in the detector are converted into phonons. These light detectors have surface areas comparable to those of the scintillating crystals they face but are made extremely thin to minimize their heat capacity and thus enhance their sensitivity to scintillation light. Because the scintillation light produced by several relevant crystals is intrinsically weak, multiple methods to optimize its detection are being developed. Strategies currently under investigation include the application of a SiO_2 coating – typically with an effective thickness of a few tens of nm – to reduce reflection (Kim et al., 2023), as well as the exploitation of the Neganov-Trofimov-Luke effect, which amplifies the thermal signal through the application of an electric field (Novati et al., 2019). The increase in the signal-to-noise ratio is crucial to reduce the background from pileup events, particularly relevant in the case of ^{100}Mo for what concerns random pairs of $2\nu\beta\beta$ events given the relatively short $2\nu\beta\beta$ half-life of this isotope ($7 \cdot 10^{18}$ yr).

The full CUPID experiment will deploy 1596 enriched Li_2MoO_4 crystals (≈250 kg of ^{100}Mo) in the existing CUORE cryostat, targeting a background index below 10^{-4} counts keV^{-1} kg^{-1} yr^{-1}and a half-life sensitivity exceeding 10^{27} yr (Alfonso et al., 2025).

6.1.6. AMoRE

A very close approach to CUPID is being pursued by AMoRE (Advanced Mo-based Rare process Experiment), where AMoRE-II (Agrawal et al., 2025b) is currently being installed at the Yemi Underground Laboratory (Yemilab, South Korea). The AMoRE-II experiment aims to search for $0\nu\beta\beta$ decay of ^{100}Mo nuclei using LMO crystals operated as scintillating bolometers. The detector will consist in an array of 423 LMO crystals 95%-enriched in ^{100}Mo for a total mass of ∼180 kg and Si wafers as light detectors (Fig. 8). The readout will be performed by metallic magnetic calorimeters (MMCs) for both heat/phonon and photon channels. MMCs provide good energy resolution and fast response times, enhancing the rejection pileup from random coincidences of two $2\nu\beta\beta$ events. The projected background is $2 \cdot 10^{-4}$ counts keV^{-1} kg^{-1} yr^{-1}in the region of interest, while the energy resolution is expected be close to 7 keV at $Q_{\beta\beta}$ (Kim et al., 2022). The sensitivity reach is $S^{0\nu}_{1/2} > 6 \cdot 10^{26}$ yr after 5 years of data collection.

AMoRE-II will profit from the experience acquired with the predecessors AMoRE-Pilot (Alenkov et al., 2019) and AMoRE-I (Agrawal et al., 2025a). Both detectors have been run in the same cryogenic infrastructure in the Yangyang Underground Laboratory (Korea). In

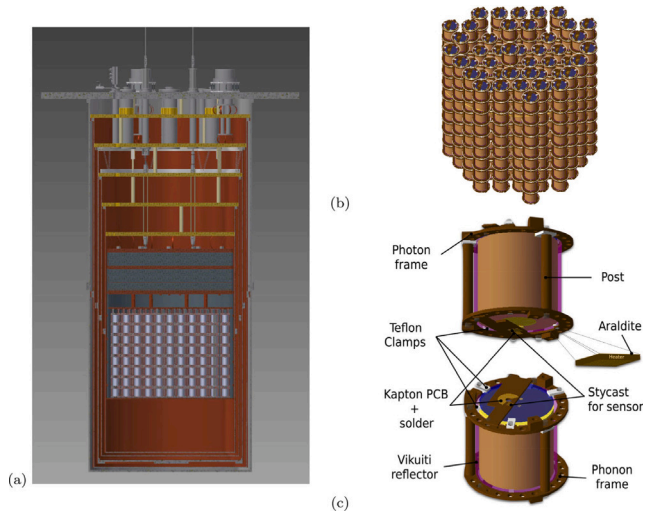


Fig. 8. Rendering of AMORE-II setup: (a) Cross-sectional view of the cryostat and installed towers; (b) detector, consisting array of 47 9-crystal towers; (c) individual detector modules.
Source: Reprinted from Ref. Agrawal et al. (2025b).

particular, AMoRE-Pilot consisted 6 crystals of $^{48depl}Ca^{100}MoO_4$ (total mass 1.9 kg), while AMoRE-I in an array of 18 crystals of enriched LMO, with a total mass of ≈6.2 kg. AMoRE-I achieved a background level of $\sim 2.5 \cdot 10^{-2}$ counts keV^{-1} kg^{-1} yr^{-1}at $Q_{\beta\beta}$, while the resolution ranged from 10 to 28 keV FWHM and recently released the limit $T^{0\nu}_{1/2} > 2.9 \cdot 10^{24}$ yr (90% C.,L.) on the $0\nu\beta\beta$ of ^{100}Mo.

6.2. Liquid scintillators

Liquid-scintillator (LS) detectors employ an organic liquid that emits fluorescence light when excited by ionizing radiation, with the collected light yield providing a measure of the deposited energy. These detectors have been widely used in nuclear and particle physics since their invention in the 1940s (Niese, 1999). Their applications cover a very broad range, from spectroscopy to calorimetry.

LS offer several advantages: they allow the construction of large, cost-effective detectors, have a fast response time of a few nanoseconds, and exhibit good linearity of light output, which can also enable particle identification. Their hydrocarbon composition ensures low-Z, low-A constituents and very low levels of radioactive contaminants, a property crucial for low-background experiments. A notable example is the Borexino detector (Agostini et al., 2018), which employed about 278 t of pseudocumene for the study of solar neutrinos and achieved ultra-low ^{238}U and ^{232}Th content, namely less than $9.4 \cdot 10^{-20}$ and $5.7 \cdot 10^{-19}$ g/g, respectively (Agostini et al., 2019). These features make liquid scintillators particularly attractive for neutrino physics, where large, ultra-clean targets are essential.

6.2.1. Loaded liquid scintillator detectors

The LS can be loaded with candidate isotopes for $0\nu\beta\beta$ searches, combining scalability, low backgrounds, and efficient light collection to enable highly sensitive experiments (Shimizu and Chen, 2019). Although these detectors do not match the precision of high-resolution technologies, by operating in ultra-low-background environments and enabling large-scale isotopic loading, loaded LS experiments are extremely effective in setting competitive limits on the $0\nu\beta\beta$ half-life.

Today, KamLAND-Zen represents the most successful example, demonstrating the ability to load almost 750 kg of xenon. Its upgrade, KamLAND2-Zen, together with SNO+ (based on tellurium), will ensure a key role for this technology in the next generation of $0\nu\beta\beta$ searches.

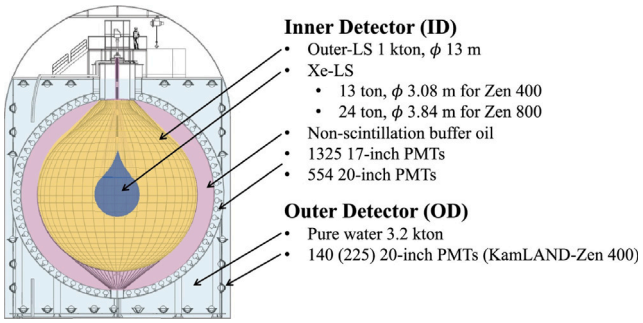


Fig. 9. Schematic view of the KamLAND-Zen detector.
Source: Reprinted from Ref. Abe et al. (2024).

6.2.2. KamLAND-Zen & KamLAND2-Zen

KamLAND-Zen (Kamioka Liquid scintillator AntiNeutrino Detector – Zero Neutrino) represented the final stage of the KamLAND program, originally designed for reactor neutrinos (Eguchi et al., 2003) (and geoneutrinos (Araki et al., 2005)), then devoted to the search for $0\nu\beta\beta$ of ^{136}Xe. The detector, located in the Kamioka mine, operated from 2011 to 2024.

KamLAND was a 1-kton liquid-scintillator detector contained in a 13-m-diameter spherical balloon instrumented with 1879 PMTs mounted on the inner surface of a stainless-steel containment tank filled with non-scintillating mineral oil (Fig. 9). The array consisted of 1325 17-inch and 554 20-inch PMTs arranged in a nearly spherical geometry to ensure uniform light collection, reliable energy reconstruction, and excellent timing performance, providing a photocathode coverage of about 34%. Low-radioactivity materials were employed to suppress external backgrounds, while regular calibration campaigns guaranteed long-term stability of gain, timing response, and dark-noise characteristics. The detector was surrounded by a 3.2-kton water-Cherenkov outer veto system, providing additional shielding and background rejection.

In the "Zen" phase (Gando et al., 2012), a 25-μm-thick transparent nylon-film inner balloon (Gando et al., 2021) was filled with LS in which xenon ∼90%-enriched in ^{136}Xe was dissolved. The xenon mass was 380 kg during Zen400 and 745 kg during Zen800. The Xe-LS was formulated by dissolving the gas into an ultra-pure organic scintillator of 82% dodecane and 18% pseudocumene by volume, with PPO added as a primary fluor at 2.4 g l^{-1} to shift the emission spectrum toward wavelengths efficiently detected by the PMTs. The density of the Xe-LS was matched to that of the surrounding scintillator to minimize mechanical stress on the balloon, while its optical properties – light yield, attenuation length, and timing – were optimized to preserve energy resolution despite xenon loading.

The exceptional radiopurity of the scintillator, at the level of 10^{-18} g/g for U and Th contaminants, was achieved through dedicated purification campaigns targeting noble gases, metal ions, and daughter products of long-lived isotopes. Energy non-linearities in the Xe-LS response were carefully characterized and corrected in the analysis.

The most recent KamLAND-Zen results, obtained using the full Zen400+Zen800 dataset – a total live time of 523.4 days, for an exposure of 2.1 ton-years of ^{136}Xe – established a lower limit $T^{0\nu}_{1/2} > 3.8 \cdot 10^{26}$ yr at 90% C. L., currently the most stringent constraint achieved in any $0\nu\beta\beta$ search. The reconstructed energy spectrum from KamLAND-Zen is shown in Fig. 10. The corresponding upper bounds on the effective Majorana neutrino mass, based on different calculations of $M_{0\nu}$, lie in the range 28–122 meV.

KamLAND is currently in its decommissioning phase in view of the upgrade to KamLAND2-Zen. KamLAND2-Zen aims at reaching a sensitivity $S^{0\nu}_{1/2} > 2 \cdot 10^{27}$ yr after 5 years of data-taking. This will be achieved by improving the energy resolution – a major limitation of this technique, as seen in Fig. 10 – from almost 10% FWHM to ∼6% in the $Q_{\beta\beta}$ region, which would also reduce the $2\nu\beta\beta$ background by a

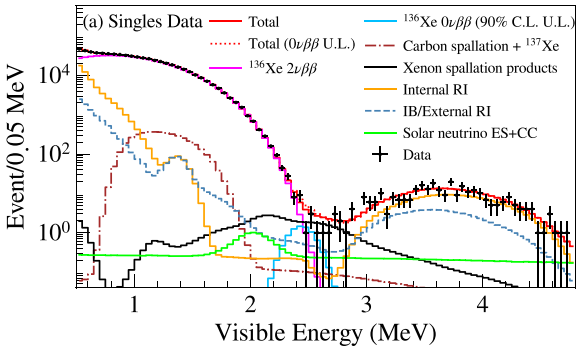


Fig. 10. Energy spectrum of the selected $\beta\beta$ candidate events inside a spherical fiducial volume of 1.57 m radius, plotted alongside the best-fit background contributions, the $2\nu\beta\beta$ decay spectrum, and the 90% C.L. upper bound on the $0\nu\beta\beta$ decay signal for the SD sample.
Source: Reprinted from Ref. Abe et al. (2025).

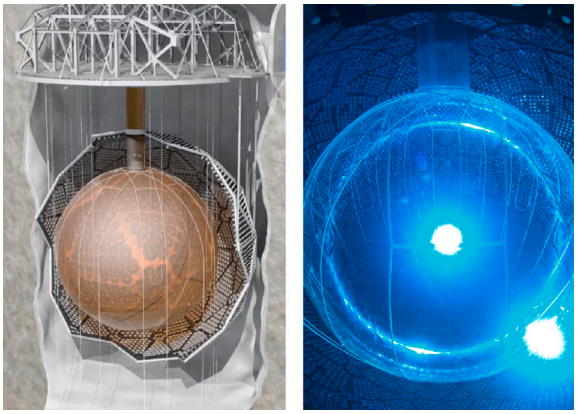


Fig. 11. Schematic view of the SNO+ detector housed within its underground cavity (left), alongside a photograph captured from inside the detector during the water phase (right).
Source: Reprinted from Ref. Albanese et al. (2021).

factor 100 (recall Fig. 3). The upgrade will be achieved by simultaneously replacing the current PMTs with higher-quantum-efficiency ones, installing light-collection Winston cone mirrors, replacing the current LS with a higher–light-yield formulation, and installing faster, virtually dead-time-free electronics (Nakane, 2025). This will be accompanied by an increase in the dissolved xenon mass to about 1 t and the implementation of background-mitigation techniques, including the replacement of the inner balloon with a scintillating one (Obara et al., 2019), which will also allow for an increase of the fiducial volume.

6.2.3. SNO+

SNO+ is a large, multipurpose experiment located at SNOLAB (Canada) in place of the SNO detector for the study of neutrino oscillations (Boger et al., 2000), and it is primarily to search for $0\nu\beta\beta$ of ^{130}Te, but it will also be a detector for solar and geo and supernova neutrinos (Albanese et al., 2021).

After an initial commissioning phase using water as the target medium, SNO+ has now been filled with 780 t of liquid scintillator. The core of the SNO+ detector is a 6-meter-radius acrylic vessel filled with LS (Fig. 11). Events occurring within the vessel are detected by 9362 inward-facing 8-inch PMTs, which are mounted on an 8.9-meter-radius steel support structure. Each PMT is equipped with a 27-cm diameter optical concentrator, providing an effective total photocoverage of 54%.

To minimize external background interference, the detector is protected by a 7000 m^3 water shielding. The water and unloaded scintillator phases serve as critical commissioning steps in preparation for tellurium loading, allowing for detector calibration and extensive background constraint measurements as components of the final scintillator mixture are gradually introduced.

The SNO+ experiment employs a liquid scintillator composed of linear alkylbenzene (LAB) loaded with 2 g l^{-1} PPO, selected for its acrylic compatibility, high optical transparency, and favorable safety characteristics. The LAB–PPO cocktail achieves an absolute light yield of approximately $1.2 \cdot 10^4$ photons MeV^{-1}, comparable to or exceeding that of traditional LS based on pseudocumene. Quenching behavior follows Birks' formalism, with particle-dependent constants, so that the analysis of the scintillation time profile enables α/β pulse-shape discrimination.

Recently, a novel loading technique was developed to dissolve tellurium into the SNO+ LS: it was found that reacting aqueous telluric acid with butanediol produces a tellurium–butanediol compound that is soluble in the SNO+ scintillator, enabling efficient deployment (Auty et al., 2023). This represents the key for the $0\nu\beta\beta$ search. In the first phase, 3900 kg of natural tellurium (0.5% loading) will be added to the scintillator, targeting a projected sensitivity of approximately $2 \cdot 10^{26}$ years (90% C. L.) over three years of data collection. Future phases will involve higher tellurium loading, with 3% loading expected to push sensitivity beyond $1 \cdot 10^{27}$ years (Albanese et al., 2021).

6.2.4. Other loaded-LS experiments

Other investigations based on dissolving different isotopes are also undergoing dedicated study. One example is ZICOS (ZIrconium Complex in Organic Scintillator) at Kamioka, which is performing feasibility tests on loading LS with zirconium to search for the $0\nu\beta\beta$ of ^{96}Zr (Fukuda et al., 2013, 2016).

A unique case in the search for $0\nu\beta\beta$ with loaded LS is that of ^{136}Xe. Xenon is itself a scintillator, so constructing a detector of pure liquid xenon effectively corresponds to a detector loaded with liquid scintillator at a concentration matching the isotopic abundance of ^{136}Xe. In this case, however, the vessel enclosing the LS must be a cryostat capable of withstanding very low temperatures, since xenon is liquid below ~165 K (at 1 atmosphere). This strategy has been followed by the XMASS experiment (also at Kamioka), a detector primarily devoted to the search of Dark Matter, but potentially applicable to the search for $0\nu\beta\beta$ (Abe et al., 2013).

6.2.5. LS as active veto

The only future major players in the search for $0\nu\beta\beta$ that will not rely on scintillation as a primary or parallel channel for detecting the emitted electrons are experiments based on HPGe detectors, where the detector acts simultaneously as source and sensor thanks to the presence of ^{76}Ge. This approach, adopted with considerable success by GERDA (Agostini et al., 2020) and Majorana Demonstrator (Arnquist et al., 2023), is now being continued by the LEGEND program. LEGEND-200 (Acharya et al., 2026), operating at LNGS since 2023 with more than 140 kg of enriched HPGe detectors, has already set a limit of $T^{0\nu}_{1/2} > 1.9 \cdot 10^{26}$ yr (90% C.,L.).

In GERDA, and even more so in LEGEND, liquid scintillator plays a crucial supporting role. The enriched-germanium arrays are operated bare in liquid argon (LAr), which simultaneously serves as coolant, shielding, and a scintillating veto for external and muon backgrounds. When ionizing radiation deposits energy in the LAr, the medium emits vacuum-ultraviolet scintillation light at 128 nm. This light is wavelength-shifted into the visible range by TPB-coated surfaces and detected by PMT (GERDA, LEGEND-200) or SiPM (LEGEND-1000) arrays surrounding the detector modules.

Although indirect for $0\nu\beta\beta$ detection, the integrated scintillation veto is a key element of LEGEND's zero-background design. The future LEGEND-1000 phase (Abgrall et al., 2021) aims for a sensitivity beyond $T^{0\nu}_{1/2} > 10^{28}$ yr, requiring background indices below 10^{-5} counts keV^{-1} kg^{-1} yr^{-1}, making the scintillating veto indispensable.

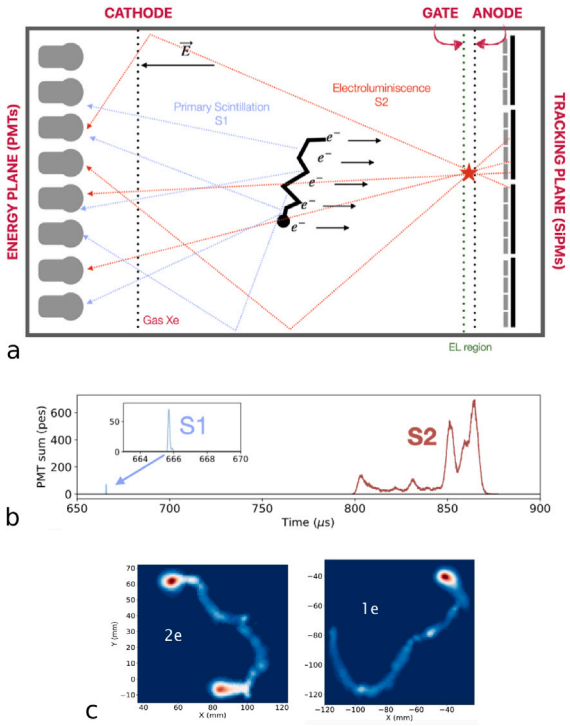


Fig. 12. (a) Operating principle of a gaseous xenon TPC with EL amplification, showing particle tracks and drifting ionization electrons. It highlights the drift and EL regions, along with the primary (S1) and secondary (S2) scintillation signals detected by the PMT energy plane and the SiPM tracking plane, used for energy measurement and 3D event reconstruction. (b) Temporal S1 and S2 signals as recorded by the PMT energy plane, (c) and spatial tracks of two events observed on the SiPM tracking plane: one produced by a single electron and the other by two electrons originating from the same initial point.
Source: Adapted from Ref. Martínez-Vara (2023).

6.3. Xenon TPCs

TPCs are a powerful technology for $0\nu\beta\beta$ searches, especially when coupled to scintillation and electroluminescence readout. A uniform electric field drifts ionization electrons toward the charge-readout system, while scintillation provides fast timing and calorimetric information. If the gas or liquid in the TPC is a scintillator, electrons accelerated in the strong electric field excite atoms, producing photons upon de-excitation; this is the case for xenon (Fig. 12).

In high-pressure gaseous xenon (HPXe) TPCs, a decay event produces prompt VUV scintillation, S1, and ionization electrons. These electrons drift to an electroluminescence region where a high electric field generates proportional secondary scintillation, S2. The S1–S2 time difference gives the absolute z-position of the interaction, while the x–y coordinates are reconstructed from the electroluminescence light distribution on the sensors. The gaseous phase preserves long ionization tracks, enabling reconstruction of the characteristic two-electron topology with terminal *energy blobs*, which provides strong background rejection. HPXe detectors also achieve energy resolutions of a few per mille because electroluminescent amplification introduces negligible noise.

In liquid xenon (LXe) TPCs, S1 and S2 signals are also produced, but the much higher density shortens track lengths to the mm scale, eliminating topological information. Moreover, recombination fluctuations in the liquid degrade energy resolution relative to HPXe. The primary advantage of LXe is scalability: multi-tonne active masses can be realized in compact geometries with established cryogenic technology, enabling the large exposures required for very long half-life sensitivities.

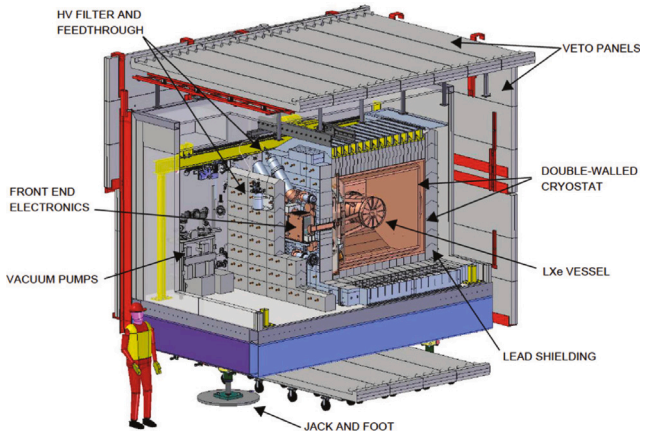


Fig. 13. The EXO-200 installation at the Waste Isolation Pilot Plant. The TPC vessel is immersed in a > 50 cm layer of HFE-7000 cryofluid, which stabilizes its temperature and shields it from external γ radiation. The cryofluid is contained in a double-walled, vacuum-insulated copper cryostat, itself surrounded by at least 25 cm of lead. The entire assembly is housed in a class-100 clean room, protected on four sides by a cosmic-ray veto system.
Source: Reprinted from Ref. Albert et al. (2014).

Both approaches have been developed and form the basis of current and next-generation $0\nu\beta\beta$ detectors. HPXe TPCs maximize energy resolution and topology-based background rejection, whereas LXe TPCs prioritize large mass and scalability. The two technologies are therefore complementary, each optimized for a different experimental strategy. The most successful $0\nu\beta\beta$ search with a xenon TPC to date is EXO. EXO-200 has been decommissioned, but its upgrade, nEXO, has been proposed, and extensive R&D is underway to characterize its expected performance and sensitivity. HPXe TPCs are being pursued by several collaborations, with active programs in the NEXT, CDEX, and AXEL experiments. Double-phase xenon TPCs, usually finding their primary application in experiments searching for Dark Matter, can also be employed for $0\nu\beta\beta$. This is the strategy pursued by PandaX-4T.

Looking further ahead, impressive active masses of order tens of tonnes are being considered for PandaX-xT and XLZD, both double-phase TPC next-to-next-generation experiments unifying expertise and resources from multiple groups, primarily from the dark-matter community. To further enhance sensitivity, these searches – aiming at half-life reaches beyond 10^{28} yr – are exploring novel strategies to improve experimental reach. An interesting recently proposed example involves a combined analysis of $0\nu\beta\beta$ to both the ground state and the first excited 0^+ state of the daughter nucleus. This approach is particularly promising for large liquid-xenon detectors, which are capable of identifying decays of ^{136}Xe to excited states with high efficiency, and could lead to an increase in sensitivity by more than a factor of two (Ding et al., 2025).

6.3.1. EXO-200 & nEXO

EXO-200 (Enriched Xenon Observatory) was located at the Waste Isolation Pilot Plant (USA) and collected data from 2011 to 2018 searching for the $0\nu\beta\beta$ of ^{136}Xe. The detector consisted of a LXe TPC filled with about 150 kg of liquid xenon enriched in ^{136}Xe at ~80% (Fig. 13). This technique enabled a low background level of ~2 counts keV^{-1} kg^{-1} yr^{-1} in the ROI, albeit with a modest energy resolution of 2.7% FWHM at $Q_{\beta\beta}$. The final result from the full dataset set a limit of $T^{0\nu}_{1/2} > 3.5 \cdot 10^{25}$ yr (90% C. L.) (Anton et al., 2019).

EXO-200 pioneered the use of LXe TPCs for $0\nu\beta\beta$; its successor, nEXO, will bring this technology to the forefront among next-generation experiments by employing 5 t of 90%-enriched xenon. Apart from the benefit of self-shielding provided by the very large LXe mass, nEXO is pursuing barium-tagging techniques to identify the Ba^{++}

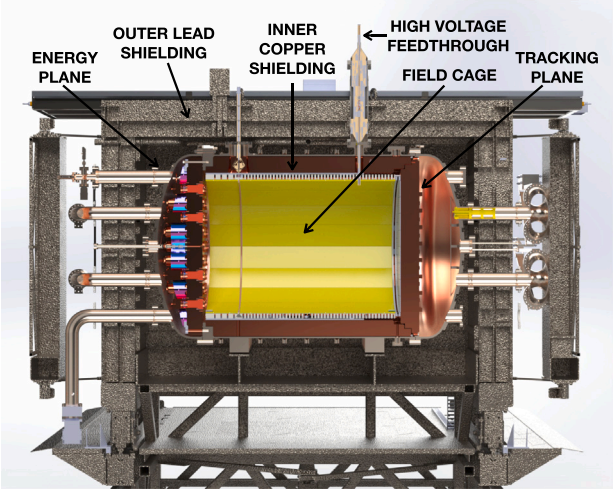


Fig. 14. Illustration of the NEXT-100 setup in Hall A of the LSC, showing the high-pressure time projection chamber, pressure vessel, internal components, and external shielding.
Source: Reprinted from Ref. C. Adams et al. (2025).

ion following the $2\nu\beta\beta$ (and $0\nu\beta\beta$) of ^{136}Xe, which would make the experiment practically background-free. For nEXO, reaching the zero-background condition requires a background index on the order of 10^{-5} counts keV^{-1} kg^{-1} yr^{-1}to achieve the impressive sensitivity $S^{0\nu}_{1/2} > 10^{28}$ yr (Adhikari et al., 2022).

6.3.2. NEXT

Among the leading experiments based on HPXe TPCs is NEXT (Neutrino Experiment with a Xenon TPC), located at the Laboratorio Subterráneo de Canfranc (Spain). The demonstrator NEXT-White, which took data from 2016 to 2021, achieved an energy resolution of ∼1% FWHM at 2.6 MeV (Novella et al., 2023) with a 4.3-kg TPC. Its design features a separated calorimetry plane based on PMTs and a tracking plane instrumented with SiPMs (Fig. 14).

The current phase, NEXT-100, commenced commissioning in 2024 (C. Adams et al., 2025). It operates with ∼80 kg xenon gas at ∼13.5 bar and is designed for ultra-low backgrounds, targeting $\sim 10^{-3}$ counts keV^{-1} kg^{-1} yr^{-1}, with a projected half-life sensitivity $S^{0\nu}_{1/2} > 6 \cdot 10^{25}$ yr after several years of live-time operation.

Beyond NEXT-100, the collaboration plans multi-tonne upgrades, NEXT-HD, and is pursuing R&D on barium tagging of the daughter ion Ba^{2+}, for a virtually background-free experiment, aiming at a sensitivity exceeding 10^{27} yr (Adams et al., 2021).

6.3.3. AXEL

The use of a HPXe TPC is at the base of the AXEL (A Xenon ElectroLuminescence) project. AXEL proposes to use multi-pixel photon counters (MPPCs) to read out the electroluminescence light, with the goal of achieving excellent energy resolution of about 0.7% FWHM at $Q_{\beta\beta}$, together with track imaging to suppress background through topological reconstruction of the event. The target resolution has already been achieved by a 180-l prototype operated with 6.8 bar of xenon, while, in order to conduct the first $0\nu\beta\beta$ search, a 1000-l-scale detector is being constructed to be run at Kamioka (Hikida et al., 2025).

6.3.4. PandaX

The PandaX-4T (Panda AND Astrophysics Xenon - 4 tonnes) detector is a dual-phase xenon TPC located in the China Jinping Underground Laboratory (CJPL) and has been operational since late 2020. The volume is filled with 3.7 t of (natural) LXe, operated at ∼178 K. The TPC features a cylindrical active region enclosed by a field cage that ensures a uniform electric field along the vertical z-axis. Photon signals are recorded by two arrays of PMTs: 169 on the top and 199 on the bottom. Physical events in the active volume generate the prompt S1 signal from scintillation light and ionized electrons, which drift upwards in the electric field and are then extracted into the gaseous xenon region, where a stronger electric field induces electroluminescence, producing delayed S2 scintillation light.

The first search for $0\nu\beta\beta$ was carried out with PandaX-II (Ni et al., 2019). PandaX-4T has conducted the initial experimental search for the $0\nu\beta\beta$ of ^{136}Xe using natural xenon, corresponding to an isotopic exposure of 44.6 kg yr, establishing a limit of $T^{0\nu}_{1/2} > 2.1 \cdot 10^{24}$ yr (90% C. L.) (Zhang et al., 2025).

The future of the project aims at the construction of the multipurpose PandaX-xT detector, with a multi-ten-tonne active target, for a wide physics program that includes the search for Dark Matter and $0\nu\beta\beta$ (Abdukerim et al., 2025). The expected sensitivity with a total target mass of 43 t is expected to range from 3 to $6{\cdot}10^{27}$ yr after 10 years of operation.

6.3.5. XLZD

The XLZD experiment (Aalbers et al., 2025) is the result of a joint effort by the XENON, LUX–ZEPLIN, and DARWIN Collaborations toward the construction of a double-phase xenon TPC capable of exploring the WIMP–nucleon interaction space down to the *neutrino fog*. Although primarily designed to play a leading role in dark matter direct detection for decades to come, XLZD's large mass, low background, and high sensitivity also enable investigations of additional physics channels, including $0\nu\beta\beta$ of ^{136}Xe. The baseline detector design features 60 t of active natural xenon, with a possible extension to 80 t. Given the immense mass and the xenon natural abundance of in ^{136}Xe, this corresponds to about 5–7 t of isotope. This would translate into a sensitivity greater than 10^{28} yr for the half-life.

6.4. Novel techniques

From the foregoing discussion, the research and development of next-generation detectors must aim to meet several, often competing, requirements: scalable detector mass, robust and low-maintenance operation over prolonged data-taking periods, and cost-effective fabrication. At the same time, these detectors must provide good energy resolution and extremely low background, minimized for both environmental and cosmogenic radioactivity. Ideally, compositional versatility to accommodate multiple $0\nu\beta\beta$ isotopes for cross-validation is also desirable.

Individually, scintillators can satisfy some of these requirements, but no single detection technique currently fulfills all of them simultaneously. Extensive research and development efforts are underway to overcome these limitations. Although this presents considerable experimental and technological challenges, the investigation of $0\nu\beta\beta$ remains both essential and compelling, offering a unique opportunity to probe physics beyond the Standard Model.

Among the various scintillator-based approaches now being explored, multiple paths are being pursued. Two particularly promising directions are nanocomposite scintillators and the use of hybrid or opaque scintillators.

6.4.1. Nanocomposite scintillators

The dispersion of nanoparticles in a host matrix of standard scintillator forms the basis of nanocomposite scintillators. Since their appearance in the early 2000s (McKigney et al., 2007), these innovative detectors have been studied for their fundamental properties and have quickly become promising tools for a wide range of technological and scientific applications (Dujardin et al., 2025). Research in this field has flourished over the years and remains highly active and rapidly evolving. These nanocomposite materials are expected to enhance the properties of the scintillators in which they are dispersed, improving

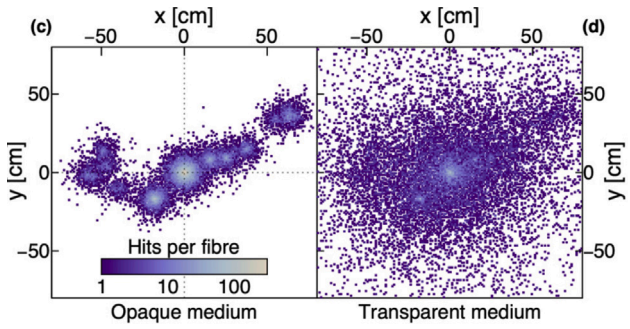


Fig. 15. Energy depositions from a simulated 1 MeV positron at the detector center, together with its annihilation gammas, are used to illustrate the LiquidO detection principle. The light collected by each fiber in a 1-cm-pitch lattice is shown for two scintillator configurations: an opaque medium with a 5 mm scattering length (left) and a fully transparent one (right). Points are color-coded by the number of photons detected per fiber. In the transparent case, unrestricted light propagation washes out the image, whereas the opaque scintillator confines light near the deposition sites, preserving event topology and enabling a sharp, high-resolution image.
Source: Reprinted from Ref. Cabrera et al. (2021).

light output and radiation interaction, while also reducing cost and enabling scalable detector sizes.

In the context of $0\nu\beta\beta$ research, nanocrystals can serve two potential roles: as wavelength shifters in large-mass liquid scintillators to improve light-collection efficiency, or as active components incorporating the $0\nu\beta\beta$ candidate isotope itself.

The former strategy has been pursued by the NuDot experiment (Gruszko et al., 2018), which aimed to exploit the temporal separation of Cherenkov and scintillation light for ∼1 MeV electrons, using fast timing to discriminate background from signal while indeed testing novel liquid-scintillator cocktails based on quantum-dot wavelength shifters. Quantum dots are semiconductor particles a few nanometers in size whose electrons can be excited and subsequently emit photoluminescence during de-excitation. NuDot was developed as a step toward the next generation of KamLAND-Zen. Beyond adding quantum dots to increase light-collection yields – with a target resolution better than 2.5% at the ^{136}Xe $Q_{\beta\beta}$– and to separate Cherenkov from scintillation light in LS already loaded with the $0\nu\beta\beta$ isotope, the quantum dots themselves could in principle be synthesized from the $0\nu\beta\beta$ candidate isotope.

Nanocrystal-based scintillators are emerging as a promising technology for future $0\nu\beta\beta$ searches (Dujardin et al., 2025). As mentioned, semiconductor quantum dots and oxide nanoparticles offer tunable optical properties, high light yield, and large Stokes shifts that minimize self-absorption, while their nm-size enables high and uniform isotope loading in liquid or solid scintillators. Recent R&D has demonstrated stable dispersions of $0\nu\beta\beta$-isotope-bearing nanoparticles such as ZrO_2, in liquid scintillators, with preserved transparency, as well as Cu-doped CdZnS/ZnS quantum-dot scintillators with enhanced radiative efficiency. These materials could combine large detector masses with improved spectral response and potentially new background-rejection capabilities through pulse-shape or timing information. The potential of this technology is very high, but significant challenges remain, including ensuring long-term optical stability, reaching competitive energy resolution, while achieving the ultra-low radiopurity required for $0\nu\beta\beta$ searches.

6.4.2. Hybrid & opaque scintillators

Scintillation light provides the energy resolution necessary for spectroscopy and for rising above the majority of radioactive backgrounds. Hybrid scintillators aim to additionally detect the Cherenkov light produced by fast particles in the medium. The separation between the prompt Cherenkov component and the delayed scintillation light enables fast timing and particle identification through their Cherenkov-to-scintillation ratio. This capability opens a wide scientific program in neutrino physics (Askins et al., 2020), including $0\nu\beta\beta$. A promising approach combines hybrid scintillators with opaque detectors.

The idea behind opaque scintillators is to confine scintillation light as close as possible to its creation point, thereby preserving detailed information about event topology. Opaque scintillators are engineered with a very short scattering length so that scintillation photons undergo repeated scattering and remain localized near their production site. The formation of *light balls* around each Compton electron is clearly visible in an opaque scintillator, whereas in a transparent medium the same pattern is almost completely smeared out, allowing a more precise reconstruction of the event (Fig. 15). Photons are then collected near their point of origin by a dense lattice of wavelength-shifting fibers within the detector. The pattern and intensity of fiber hits indicate where the light was produced, enabling accurate reconstruction of both the topology and the deposited energy.

The opacization of the LS can be achieved by doping with various compounds, a process that also opens the possibility of new physics measurements; the dopant may include $0\nu\beta\beta$ candidate isotopes. The LiquidO Collaboration was the first to propose searching for double weak decays by exploiting distinct event topologies in opaque media, enabling studies of double-electron and double-positron channels (Cabrera et al., 2018).

The combination of hybrid and opaque scintillation techniques thus offers strong background suppression, high isotope-loading capability, and the ability to reconstruct complex β^+ event signatures, making it well suited for probing both two-neutrino and neutrinoless double-positron decay modes ($2\nu\beta^+\beta^+$ and $0\nu\beta^+\beta^+$). The NuDoubt++ (Neutrino Double beta plus plus) experiment plans to merge hybrid and opaque scintillator technologies to enable highly sensitive searches for $0\nu\beta^+\beta^+$. The design of a proof-of-concept detector with a 10-kg fiducial volume loaded with ^{78}Kr – the $0\nu\beta^+\beta^+$ candidate isotopes are not those listed in Table 1 – aims to demonstrate the potential of this strategy, targeting an energy resolution of 2.2% in the ROI at ∼3 MeV and a background level of $2 \cdot 10^{-5}$ counts keV^{-1} kg^{-1} yr^{-1} (Böhles et al., 2025).

7. Conclusions

The search for $0\nu\beta\beta$ is a crucial probe of physics beyond the Standard Model and a benchmark to investigate neutrino properties. Over decades of development, experiments based on different techniques have succeeded one another, and today sensitivities on the half-lives greater than 10^{26} yr have been achieved. Despite the diversity of approaches currently employed in $0\nu\beta\beta$ searches, scintillation plays a central and unifying role. A large fraction of present and upcoming experiments relies on either solid or liquid scintillators as the primary detection medium, often exploiting dual-channel light+heat readout as scintillating bolometers to achieve powerful particle-identification capabilities and significant background suppression. Xenon-based detectors also allow for the simultaneous collection of scintillation and ionization charge. Even experiments that do not use scintillators to detect the $0\nu\beta\beta$ signal itself employ them in active veto systems, which are critical for reaching the required background levels.

At the same time, rapid technological progress is enabling entirely new approaches. Advances in crystal growth and purification, high-loadable liquid scintillators, cryogenic light sensors, and fast or quantum-enhanced readout technologies are expanding the landscape of available options. Novel scintillating materials and hybrid detection schemes promise improvements in energy resolution, radiopurity, and scalability, pushing the sensitivity of next-generation experiments toward a full exploration of the Inverted Hierarchy regime. The target of half-lives larger than 10^{27}–10^{28} yr will impose extremely stringent requirements for zero background in the ROI over year-long exposures and tonne-scale detector masses. In this evolving context, scintillators will continue to play a pivotal role, substantially contributing to the worldwide effort to observe – or rule out – $0\nu\beta\beta$.

CRediT authorship contribution statement

S. Dell'Oro: Writing – review & editing, Writing – original draft. **L. Gironi:** Writing – review & editing, Writing – original draft.

Declaration of Generative AI and AI-assisted technologies in the writing process

During the preparation of this work the authors used ChatGPT in order to improve the readability of the paper. After using this tool/service, the authors reviewed and edited the content as needed and take full responsibility for the content of the published article.

Declaration of competing interest

The authors declare that they have no known competing financial interests or personal relationships that could have appeared to influence the work reported in this paper.

Data availability

No data was used for the research described in the article.

References

Aalbers, J., et al., XLZD Collaboration Collaboration, 2025. Neutrinoless double beta decay sensitivity of the XLZD rare event observatory. J. Phys. G 52 (4), 045102. http://dx.doi.org/10.1088/1361-6471/adb900.

Abdukerim, A., et al., PandaX Collaboration Collaboration, 2025. PandaX-xT—A deep underground multi-ten-tonne liquid xenon observatory. Sci. China Phys. Mech. Astron. 68 (2), 221011. http://dx.doi.org/10.1007/s11433-024-2539-y.

Abe, K., et al., 2013. XMASS detector. Nucl. Instrum. Methods A 716, 78–85. http://dx.doi.org/10.1016/j.nima.2013.03.059.

Abe, K., et al., Hyper-Kamiokande Collaboration Collaboration, 2015. Physics potential of a long-baseline neutrino oscillation experiment using a J-PARC neutrino beam and Hyper-Kamiokande. Prog. Theor. Exp. Phys. 2015, 053C02. http://dx.doi.org/10.1093/ptep/ptv061.

Abe, S., et al., 2024. Search for charged excited states of dark matter with KamLAND-Zen. Phys. Lett. B 855, 138846. http://dx.doi.org/10.1016/j.physletb.2024.138846.

Abe, S., et al., KamLAND-Zen Collaboration Collaboration, 2025. Search for Majorana neutrinos with the complete KamLAND-Zen dataset. Phys. Rev. Lett. 135, 262501. http://dx.doi.org/10.1103/jkf6-48j8.

Abgrall, N., et al., LEGEND Collaboration Collaboration, 2021. LEGEND-1000 preconceptual design report.

Abi, B., et al., DUNE Collaboration Collaboration, 2020. Long-baseline neutrino oscillation physics potential of the DUNE experiment. Eur. Phys. J. C 80 (10), 978. http://dx.doi.org/10.1140/epjc/s10052-020-08456-z.

Abusleme, A., et al., JUNO Collaboration Collaboration, 2022. JUNO physics and detector. Prog. Part. Nucl. Phys. 123, 103927. http://dx.doi.org/10.1016/j.ppnp.2021.103927.

Acharya, H., et al., LEGEND Collaboration Collaboration, 2026. First results on the search for Lepton number violating neutrinoless double beta decay with the LEGEND-200 experiment. Phys. Rev. Lett. 136, 022701. http://dx.doi.org/10.1103/25tk-nctn.

Adams, C., et al., NEXT Collaboration Collaboration, 2021. Sensitivity of a tonne-scale NEXT detector for neutrinoless double beta decay searches. J. High Energy Phys. 2021 (08), 164. http://dx.doi.org/10.1007/JHEP08(2021)164.

Adams, D.Q., et al., CUORE Collaboration Collaboration, 2024. Data-driven background model for the CUORE experiment. Phys. Rev. D 110, 052003. http://dx.doi.org/10.1103/PhysRevD.110.052003.

Adams, D.Q., et al., CUORE Collaboration Collaboration, 2025. Constraints on Lepton number violation with the 2 tonne·yr CUORE dataset. Science 390, 1029–1032. http://dx.doi.org/10.1126/science.adp6474.

Adams, C., et al., NEXT Collaboration Collaboration, 2025. The NEXT-100 detector. URL https://arxiv.org/abs/2505.17848.

Adhikari, G., et al., 2022. nEXO: neutrinoless double beta decay search beyond 10^{28} year half-life sensitivity. J. Phys. G 49, 015104. http://dx.doi.org/10.1088/1361-6471/ac3631.

Agostini, M., Benato, G., Detwiler, J.A., Menéndez, J., Vissani, F., 2023. Toward the discovery of matter creation with neutrinoless $\beta\beta$ decay. Rev. Mod. Phys. 95 (2), 025002. http://dx.doi.org/10.1103/RevModPhys.95.025002.

Agostini, M., et al., BOREXINO Collaboration Collaboration, 2018. Comprehensive measurement of *pp*-chain solar neutrinos. Nature 562 (7728), 505–510. http://dx.doi.org/10.1038/s41586-018-0624-y.

Agostini, M., et al., Borexino Collaboration, 2019. First simultaneous precision spectroscopy of *pp*, ^{7}Be, and *pep* solar neutrinos with Borexino phase-II. Phys. Rev. D 100 (8), 082004. http://dx.doi.org/10.1103/PhysRevD.100.082004.

Agostini, M., et al., GERDA Collaboration Collaboration, 2020. Final results of GERDA on the search for neutrinoless double-β decay. Phys. Rev. Lett. 125 (25), 252502. http://dx.doi.org/10.1103/PhysRevLett.125.252502.

Agrawal, A., et al., AMoRE Collaboration Collaboration, 2025a. Improved limit on neutrinoless double beta decay of ^{100}Mo from AMoRE-I. Phys. Rev. Lett. 134, 082501. http://dx.doi.org/10.1103/PhysRevLett.134.082501.

Agrawal, A., et al., AMoRE Collaboration Collaboration, 2025b. Projected background and sensitivity of AMoRE-II. Eur. Phys. J. C 85 (9), http://dx.doi.org/10.1140/epjc/s10052-024-13516-9.

Ajimura, S., et al., CANDLES Collaboration Collaboration, 2021. Low background measurement in CANDLES-III for studying the neutrino-less double beta decay of ^{48}Ca. Phys. Rev. D 103 (9), 092008. http://dx.doi.org/10.1103/PhysRevD.103.092008.

Albanese, V., et al., SNO+ Collaboration Collaboration, 2021. The SNO+ experiment. J. Instrum. 16 (08), P08059. http://dx.doi.org/10.1088/1748-0221/16/08/P08059.

Albert, J.B., et al., EXO Collaboration Collaboration, 2014. Improved measurement of the $2\nu\beta\beta$ half-life of ^{136}xe with the EXO-200 detector. Phys. Rev. C 89, 015502. http://dx.doi.org/10.1103/PhysRevC.89.015502.

Alenkov, V., et al., 2019. First results from the AMoRE-Pilot neutrinoless double beta decay experiment. Eur. Phys. J. C 79 (9), 791. http://dx.doi.org/10.1140/epjc/s10052-019-7279-1.

Alfonso, K., et al., 2023. Twelve-crystal prototype of Li_2MoO_4 scintillating bolometers for CUPID and CROSS experiments. J. Instrum. 18 (06), P06018. http://dx.doi.org/10.1088/1748-0221/18/06/P06018.

Alfonso, K., et al., CUPID Collaboration Collaboration, 2025. CUPID, the cuore upgrade with particle identification. Eur. Phys. J. C 85 (737), http://dx.doi.org/10.1140/epjc/s10052-025-14352-1.

Anton, G., et al., EXO-200 Collaboration Collaboration, 2019. Search for neutrinoless double-β decay with the complete EXO-200 dataset. Phys. Rev. Lett. 123 (16), 161802. http://dx.doi.org/10.1103/PhysRevLett.123.161802.

Araki, T., et al., 2005. Experimental investigation of geologically produced antineutrinos with KamLAND. Nature 436, 499–503. http://dx.doi.org/10.1038/nature03980.

Arnaboldi, C., et al., 2010. $CdWO_4$ scintillating bolometer for double beta decay: Light and heat anticorrelation, light yield and quenching factors. Astropart. Phys. 34 (3), 143–150. http://dx.doi.org/10.1016/j.astropartphys.2010.06.009.

Arnquist, I.J., et al., Majorana Collaboration Collaboration, 2023. Final result of the majorana demonstrator's search for neutrinoless double-β decay in ^{76}Ge. Phys. Rev. Lett. 130 (6), 062501. http://dx.doi.org/10.1103/PhysRevLett.130.062501.

Askins, M., et al., THEIA Collaboration Collaboration, 2020. THEIA: an advanced optical neutrino detector. Eur. Phys. J. C 80 (5), 416. http://dx.doi.org/10.1140/epjc/s10052-020-7977-8.

Augier, C., et al., CUPID-Mo Collaboration Collaboration, 2022. Final results on the $0\nu\beta\beta$ decay half-life limit of ^{100}Mo from the CUPID-Mo experiment. Eur. Phys. J. C 82 (11), 1033. http://dx.doi.org/10.1140/epjc/s10052-022-10942-5.

Auty, D.J., et al., 2023. A method to load tellurium in liquid scintillator for the study of neutrinoless double beta decay. Nucl. Instrum. Methods A 1051, 168204. http://dx.doi.org/10.1016/j.nima.2023.168204.

Azzolini, O., et al., CUPID-0 Collaboration Collaboration, 2022a. Final result on the neutrinoless double beta decay of ^{82}Se with CUPID-0. Phys. Rev. Lett. 129 (11), 111801. http://dx.doi.org/10.1103/PhysRevLett.129.111801.

Azzolini, O., et al., 2022b. Final result on the neutrinoless double beta decay of ^{82}Se with CUPID-0. Phys. Rev. Lett. 129, 111801. http://dx.doi.org/10.1103/PhysRevLett.129.111801.

Barabash, A.S., 2011. Double beta decay: Historical review of 75 years of research. Phys. At. Nucl. 74, 603–613. http://dx.doi.org/10.1134/S1063778811030070.

Barabash, A.S., et al., 2011. Low background detector with enriched $^{116}CdWO_4$ crystal scintillators to search for double β decay of ^{116}Cd. J. Instrum. 6 (08), P08011. http://dx.doi.org/10.1088/1748-0221/6/08/P08011.

Barabash, A.S., et al., 2018. Final results of the aurora experiment to study 2β decay of ^{116}Cd with enriched $^{116}CdWO_4$ crystal scintillators. Phys. Rev. D 98 (9), 092007. http://dx.doi.org/10.1103/PhysRevD.98.092007.

Bethe, H., Peierls, R., 1934. The "neutrino". Nature 133, 532. http://dx.doi.org/10.1038/133532a0.

Biller, S.D., 2013. Probing Majorana neutrinos in the regime of the normal mass hierarchy. Phys. Rev. D 87 (7), 071301. http://dx.doi.org/10.1103/PhysRevD.87.071301.

Birks, J.B., 1951. Scintillations from organic crystals: Specific fluorescence and relative response to different radiations. Proc. Phys. Soc. A 64 (10), 874. http://dx.doi.org/10.1088/0370-1298/64/10/303.

Boger, J., et al., SNO Collaboration Collaboration, 2000. The Sudbury neutrino observatory. Nucl. Instrum. Methods A 449, 172–207. http://dx.doi.org/10.1016/S0168-9002(99)01469-2.

Böhles, M., et al., 2025. Combining hybrid and opaque scintillator techniques in the search for double beta plus decays. Eur. Phys. J. C 85, 121. http://dx.doi.org/10.1140/epjc/s10052-025-13847-1.

Bonvicini, V., Capelli, S., Cremonesi, O., Cucciati, G., Gironi, L., Pavan, M., Previtali, E., Sisti, M., 2014. A flexible scintillation light apparatus for rare event searches. Eur. Phys. J. C 74 (11), 3151. http://dx.doi.org/10.1140/epjc/s10052-014-3151-5.

Brofferio, C., Dell'Oro, S., 2018. Contributed review: The saga of neutrinoless double beta decay search with TeO_2 thermal detectors. Rev. Sci. Instrum. 89 (12), 121502. http://dx.doi.org/10.1063/1.5031485.

Cabrera, A., et al., LiquidO Collaboration Collaboration, 2018. Physics potential of the novel liquido technique. In: Presented at Neutrino Oscillation Workshop. NOW-2018, http://dx.doi.org/10.5281/zenodo.7576322.

Cabrera, A., et al., LiquidO Consortium Collaboration, 2021. Neutrino physics with an opaque detector. Commun. Phys. 4 (273), http://dx.doi.org/10.1038/s42005-021-00763-5.

Capozzi, F., Giarè, W., Lisi, E., Marrone, A., Melchiorri, A., Palazzo, A., 2025. Neutrino masses and mixing: Entering the era of subpercent precision. Phys. Rev. D 111, 093006. http://dx.doi.org/10.1103/PhysRevD.111.093006.

Cowan, C.L., Reines, F., Harrison, F.B., Kruse, H.W., McGuire, A.D., 1956. Detection of the free neutrino: A confirmation. Science 124, 103–104. http://dx.doi.org/10.1126/science.124.3212.103.

Davis, Jr., R., Harmer, D.S., Hoffman, K.C., 1968. Search for neutrinos from the sun. Phys. Rev. Lett. 20, 1205–1209. http://dx.doi.org/10.1103/PhysRevLett.20.1205.

Dell'Oro, S., Marcocci, S., Viel, M., Vissani, F., 2016. Neutrinoless double beta decay: 2015 review. Adv. High Energy Phys. 2016, 2162659. http://dx.doi.org/10.1155/2016/2162659.

Ding, C.R., Han, K., Wang, S.B., Yao, J.M., 2025. Enhancing the sensitivity of neutrinoless double beta decays via combined multi-transition analysis.

Dujardin, C., et al., 2025. Inorganic nanoscintillators: Current trends and future perspectives. Adv. Opt. Mater. 13 (12), 2402739. http://dx.doi.org/10.1002/adom.202402739.

Eguchi, K., et al., KamLAND Collaboration Collaboration, 2003. First results from KamLAND: Evidence for reactor anti-neutrino disappearance. Phys. Rev. Lett. 90, 021802. http://dx.doi.org/10.1103/PhysRevLett.90.021802.

Fermi, E., 1934. Trends to a theory of β radiation (in Italian). Nuovo Cim. 1–19. http://dx.doi.org/10.1007/BF02959820.

Fireman, E.L., 1948. Artificial radioactive substances. Phys. Rev. 74, 1238. http://dx.doi.org/10.1103/PhysRev.74.1201.

Fukuda, Y., Moriyama, S., Ogawa, I., 2013. Development of liquid scintillator containing a zirconium complex for neutrinoless double beta decay experiment. Nucl. Instrum. Methods A 732, 397–402. http://dx.doi.org/10.1016/j.nima.2013.06.043.

Fukuda, Y., Takahiro, G., Moriyama, S., Ogawa, I., 2016. Development of a liquid scintillator containing a zirconium β-keto ester complex for the ZICOS experiment. Nucl. Part. Phys. Proc. 273–275, 2615–2617. http://dx.doi.org/10.1016/j.nuclphysbps.2015.10.007.

Fukugita, M., Yanagida, T., 1986. Baryogenesis without grand unification. Phys. Lett. B 174, 45. http://dx.doi.org/10.1016/0370-2693(86)91126-3.

Furry, W.H., 1939. On transition probabilities in double beta-disintegration. Phys. Rev. 56, 1184–1193. http://dx.doi.org/10.1103/PhysRev.56.1184.

Gando, A., et al., KamLAND-Zen Collaboration Collaboration, 2012. Measurement of the double-β decay half-life of ^{136}Xe with the KamLAND-Zen experiment. Phys. Rev. C 85, 045504. http://dx.doi.org/10.1103/PhysRevC.85.045504.

Gando, Y., et al., KamLAND-Zen Collaboration Collaboration, 2021. The nylon balloon for xenon loaded liquid scintillator in KamLAND-Zen 800 neutrinoless double-beta decay search experiment. J. Instrum. 16 (08), P08023. http://dx.doi.org/10.1088/1748-0221/16/08/P08023.

Gironi, L., et al., 2010. Performance of $ZnMoO_4$ crystal as cryogenic scintillating bolometer to search for double beta decay of molybdenum. J. Instrum. 5 (11), P11007. http://dx.doi.org/10.1088/1748-0221/5/11/P11007.

Goeppert-Mayer, M., 1935. Double beta-disintegration. Phys. Rev. 48, 512–516. http://dx.doi.org/10.1103/PhysRev.48.512.

Gómez-Cadenas, J.J., Martìn-Albo, J., Menéndez, J., Mezzetto, M., Monrabal, F., Sorel, M., 2023. The search for neutrinoless double-beta decay. Riv. Nuovo Cim. 46 (10), 619–692. http://dx.doi.org/10.1007/s40766-023-00049-2.

Gruszko, J., et al., 2018. NuDot: Double-beta decay with direction reconstruction in liquid scintillator. In: Presented at the XXVIII International Conference on Neutrino Physics and Astrophysics. http://dx.doi.org/10.5281/zenodo.1300693.

Hikida, J., et al., 2025. AXEL: High-pressure xenon gas TPC for neutrinoless double beta decay search. Nucl. Instrum. Methods A 1080, 170706. http://dx.doi.org/10.1016/j.nima.2025.170706.

Iida, T., et al., 2021. The energy calibration system for CANDLES using (n, γ) reaction. Nucl. Instrum. Methods A 986, 164727. http://dx.doi.org/10.1016/j.nima.2020.164727.

Kim, W.T., et al., 2022. Optimization of cryogenic calorimetric detection with lithium molybdate crystals for AMoRE-II experiments. J. Instrum. 17 (07), P07034. http://dx.doi.org/10.1088/1748-0221/17/07/P07034.

Kim, M.B., et al., 2023. Large area light detectors with MMC readouts. IEEE Trans. Appl. Supercond. 33 (5), 1–5. http://dx.doi.org/10.1109/TASC.2023.3263333.

Kotila, J., Iachello, F., 2012. Phase space factors for double-β decay. Phys. Rev. C 85, 034316. http://dx.doi.org/10.1103/PhysRevC.85.034316.

Majorana, E., 1937. Theory of the symmetry of electrons and positrons (in Italian). Nuovo Cim. 14, 171–184. http://dx.doi.org/10.1007/BF02961314.

Martínez-Vara, M., 2023. NEXT, a neutrinoless double beta decay experiment. Proc. Sci. EPS-HEP2023, 169. http://dx.doi.org/10.22323/1.449.0169.

McKigney, E.A., et al., 2007. Nanocomposite scintillators for radiation detection and nuclear spectroscopy. Nucl. Instrum. Methods A 579 (1), 15–18. http://dx.doi.org/10.1016/j.nima.2007.04.004.

Nakane, J., 2025. New detector development and performance evaluation for KamLAND2-Zen. Nucl. Instrum. Methods A http://dx.doi.org/10.1016/j.nima.2025.170850.

Ni, K., et al., PandaX Collaboration Collaboration, 2019. Searching for neutrino-less double beta decay of ^{136}Xe with PandaX-II liquid xenon detector. Chin. Phys. C 43 (11), 113001. http://dx.doi.org/10.1088/1674-1137/43/11/113001.

Niese, S., 1999. The discovery of organic solid and liquid scintillators by H. Kallmann and L. Herforth 50 years ago. J. Radioanal. Nucl. Chem. 241 (2), 499–501. http://dx.doi.org/10.1007/BF02347204.

Novati, V., et al., 2019. Charge-to-heat transducers exploiting the Neganov-Trofimov-Luke effect for light detection in rare-event searches. Nucl. Instrum. Methods A 940, 320–327. http://dx.doi.org/10.1016/j.nima.2019.06.044.

Novella, P., et al., 2023. Demonstration of neutrinoless double beta decay searches in gaseous xenon with NEXT. J. High Energy Phys. 9, 190. http://dx.doi.org/10.1007/JHEP09(2023)190.

Obara, S., Gando, Y., Ishidoshiro, K., 2019. Scintillation balloon for neutrinoless double-beta decay search with liquid scintillator detectors. Prog. Part. Nucl. Phys. 2019 (7), 073H01. http://dx.doi.org/10.1093/ptep/ptz064.

Ogawa, I., et al., 2023. Laser isotope separation to study for the neutrino-less double beta decay of ^{48}Ca. J. Phys. Conf. Ser. 2586 (1), 012136. http://dx.doi.org/10.1088/1742-6596/2586/1/012136.

Pauli, W.E., 1930. Open letter to the group of radioactive people at the Gauverein meeting in Tübingen (in German). (unpublished).

Pontecorvo, B., 1957. Mesonium and anti-mesonium. Sov. Phys. jeTP 6, 429; 1957. Zh. Eksp. Teor. Fiz. 33, 549.

Racah, G., 1937. On the symmetry of particle and antiparticle (in Italian). Nuovo Cim. 14, 322–328. http://dx.doi.org/10.1007/BF02961321.

Reines, F., Cowan, C.L., 1956. The neutrino. Nature 178, 446–449. http://dx.doi.org/10.1038/178446a0.

Shimizu, I., Chen, M., 2019. Double beta decay experiments with loaded liquid scintillator. Front. Phys. 7, 33. http://dx.doi.org/10.3389/fphy.2019.00033.

Tetsuno, K., et al., CANDLES collaboration and low temperature group Collaboration, 2020. Status of ^{48}Ca double beta decay search and its future prospect in CANDLES. J. Phys. Conf. Ser. 1468 (1), 012132. http://dx.doi.org/10.1088/1742-6596/1468/1/012132.

Tretyak, V.I., 2010. Semi-empirical calculation of quenching factors for ions in scintillators. Astropart. Phys. 33, 40–53. http://dx.doi.org/10.1016/j.astropartphys.2009.11.002.

Umehara, S., et al., 2008. Neutrino-less double-beta decay of ^{48} studied by CaF_2(eu) scintillators. Phys. Rev. C 78, 058501. http://dx.doi.org/10.1103/PhysRevC.78.058501.

Vissani, F., 1999. Signal of neutrinoless double beta decay, neutrino spectrum and oscillation scenarios. J. High Energy Phys. 06, 022. http://dx.doi.org/10.1088/1126-6708/1999/06/022.

Yoshida, S., et al., 2009. Ultra-violet wavelength shift for undoped CaF_2 scintillation detector by two phase of liquid scintillator system in CANDLES. Nucl. Instrum. Methods A 601 (3), 282–293. http://dx.doi.org/10.1016/j.nima.2008.12.190.

Zhang, S., et al., 2025. Searching for neutrinoless double-beta decay of 136Xe with PandaX-4T. Sci. Bull. 70 (11), 1779–1785. http://dx.doi.org/10.1016/j.scib.2025.03.009.